Reconstructing the Salgar 2015 Flash Flood Using Radar Retrievals and a Conceptual Modeling Framework: A Basis for a Better Flood Generating Mechanisms Discrimination

Nicolás Velásquez [1,2], Carlos D. Hoyos [1,2], Jaime I. Vélez [1], and Esneider Zapata [2]

[1]Universidad Nacional de Colombia, Sede Medellín, Facultad de Minas, Departamento de Geociencias y Medio Ambiente
[2]Sistema de Alerta Temprana de Medellín y el Valle de Aburrá (SIATA)

Correspondence to: Nicolás Velásquez (nvelasqg@unal.edu.co)

Abstract. ~~Flash floods associated with severe precipitation events are highly destructive, often resulting in significant human and economic losses. Due to their nature, flash floods tend to occur in medium to small basins located within complex high mountainous regions. In the Colombian Andean region these basins are common, with the aggravating factor that the vulnerability is considerably high due to the presence of important human settlements frequently occupying floodplains and other flash-flood prone areas.~~ During May 18 of 2015, severe rainfall ~~generated~~ triggered a flash flood in the municipality of Salgar, ~~in La Liboriana basin~~ located in the northwestern Colombian Andes~~, resulting in more than 100 human casualties and significant economic losses~~. This work aims to reconstruct the ~~2015 La Liboriana~~ main features of the flash flood to understand better the hydrological processes ~~that took place during the event and to serve as a proof of concept for the development of a flash flood guidance low-cost tool when information is scarce. Radar QPE~~modulating the event occurrence. Radar quantitative precipitation estimates (QPE), satellite data, and post-event field visits are used to reconstruct the Salgar flash flood addressing the relationship between rainfall spatio-temporal structure, soil moisture, and runoff generation during successive rainfall events, using a conceptual modeling framework including land-slide and hydraulic sub-models. The ~~hydrological model includes the addition of~~ hydrologic model includes virtual tracers to explore the role of runoff and subsurface flow, as well as the relative importance of convective and stratiform precipitation in flash flood generation. ~~The~~ In spite of potential shortcomings, the modeling results allow an assessment of the impact of the interactions between runoff, subsurface flow, and convective-stratiform rainfall ~~allows a better understanding of~~ on the short-term hydrological mechanisms leading to the flash flood event. The overall methodology reproduces considerably well the magnitude and timing

of La Liboriana flash flood discharge peak, as well as the areas of ~~regional land-slide~~ landslide occurrence and flood spots~~location~~, with some limitations due to the ~~available spatial scale of the~~ digital elevation model spatial resolution. Simulation results indicate that the flash-flood and the regional land-slide features were strongly influenced by the antecedent rainfall associated with a northeasterly stratiform event that recharged the gravitational and capillary storages ~~. The hydrologic~~ within the model. The simulation shows that the antecedent ~~event set wet conditions in~~ rainfall event moistens the entire basin before the occurrence of the flash flood event, ~~governing~~ modulating as well the streamflow during the flash flood event. Evidence suggests that the spatial structure of the rainfall is at least as important as the geomorphological features of the basin ~~regulating the generation~~ in regulating the occurrence of flash flood events. ~~Results also suggest that the described model-based tool is useful for policy-makers not only for short-term decisions in the context of an early warning system but also as a planning resource for long-term risk management.~~

1   Introduction

Flash floods are regarded as one of the most destructive hydrological hazards resulting in considerable loss of human life and high costs due to infrastructure ~~damages (Roux et al., 2011; Gruntfest and Handmer, 2001)~~ ~~.~~ damage (Roux et al., 2011; Gruntfest and Handmer, 2001). Among all different types of floods, Jonkman (2005) shows that flash floods result in the highest average mortality rate per event (3.62%), almost ten times larger than the mortality rate for river floods. Flash floods are usually described as rapidly rising water level events happening in steep streams and rivers, associated with short-term, very intense convective precipitation systems, or orographically forced rainfall events over highly saturated land surfaces and steep terrains (Šálek et al., 2006; Llasat et al., 2016; Douinot et al., 2016). Convective precipitation episodes often feature high ~~intensities, short durations~~intensity, short duration, and relatively reduced spatial coverage (Houze, 2004). ~~Jonkman (2005), based on information from the International Disaster Database, maintained by the United States Office for Foreign Disaster Assistance and the Center for Research on the Epidemiology of Disasters in Brussels, shows that between 1975 and 2001 a total of 1816 worldwide freshwater flood events killed over 175, 000 persons and affected more than 2.2 billion people. These events not only caused human and economic losses but also damages to ecosystems and loss of historical and cultural values. Among all different types of floods, Jonkman (2005) shows that flash floods result in the highest average mortality rate per event (3.62%), almost ten times larger than the mortality rate for river floods.~~

~~Several studies assess the role of rainfall, geomorphological features and soil conditions on flash floods occurrence from different points of view. Wu and Sidle (1995) highlight~~ Several authors have assessed the role of the geological and geomorphological features of the catchment, soil type, soil moisture conditions, and the spatio-temporal structure of rainfall on flash flood occurrence, trying to

identify the leading causative mechanisms of this hazard (Merz and Blöschl, 2003). Adamovic et al. (2016) and Vannier et al. (2016) tried to understand the governing processes of flash floods from the geological formation of the basin with mixed results. Wu and Sidle (1995) emphasize the role of the topography, ground cover, and groundwater in the occurrence of shallow landslides and associated debris flows. ~~Merz and Blöschl (2003) highlighted the importance of understanding the physical processes giving rise to floods of a certain probability of occurrence and proposed a framework, from a catchment perspective, for identifying causative mechanisms of inundations and the viability for a large number of episodes and basins~~ Due to their rapid nature, flash floods are more likely to occur in small and steep basins (Younis et al., 2008); many authors have assessed the influence of hills and stream slopes suggesting the slopes of the hills are significantly more important for flash floods occurrence and magnitude than the slope of the stream (Šálek et al., 2006; Roux et al., 2011; Yatheendradas et al., 2008). Rodriguez-Blanco et al. (2012) analyzed fifty-four flash flood episodes in Spain and determined that antecedent soil moisture conditions play a vital role in runoff production. Castillo et al. (2003), using a modeling approach, also suggested an important flash flood occurrence dependence on antecedent moisture conditions. Aronica et al. (2012) used spatial and statistical analysis to reconstruct landslides and deposits, finding a connection between flash flood occurrence and soil moisture antecedent conditions.

The fact that small basins are more prone to flash floods increases their intrinsic physical and measurement uncertainty (Wagener et al., 2007), difficulting their prediction (Hardy et al., 2016; Ruiz-Villanueva et al., 2013; Yama, and underlining the need for high spatio-temporal resolution precipitation data (Norbiato et al., 2008). Given the critical role of precipitation, some authors follow a climatological approximation to assess the recurrence of flash floods in particular regions~~and study the different~~, focusing on the atmospheric causative mechanisms. ~~These studies have evidenced the need to incorporate global and regional climatological conditions and variability in local risk reduction.~~ For example, Kahana et al. (2002) examined the extent to which floods in the Negev Desert are the outcome of ~~distinct~~ climatological synoptic-scale features finding that about 80% of the events can be linked to distinct synoptic ~~types characterized by the prevailing atmospheric~~ conditions days prior the flood events. Schumacher and Johnson (2005) studied extreme rain events associated with flash flooding in the United States over a 3-yr period using the national radar reflectivity composite data ~~are~~ to examine the structure and evolution of each extreme rain events. The use of radar data to study flash flood generating storms is vital for understanding and forecasting these events (National Research Council 1996). Schumacher and Johnson (2005) found that 65% of the total number of episodes are associated with mesoscale convective systems (MCSs), with two recurrent patterns of organization: the existence of training convective elements and the generation of quasi-stationary areas of convection with stratiform rainfall downstream. Fragoso et al. (2012) analyzed storm characteristics and required rainfall conditions for flash flood occurrence at Madeira (Portugal), and their results suggest an essential role

of global climate patterns (North Atlantic Oscillation -NAO- forcing) and also local forcing (oro-

95 graphic features) in the triggering of such events. ~~Piper et al. (2016) examined the critical elements of flash flood triggering storms following a statistical approach, finding an essential role of stationary convective cores. Gochis et al. (2015) studied the great Colorado flood of 2013, documenting not only the meteorological conditions but also the climatological ones responsible for producing the observed widespread destruction, associating them with the potential for sustaining a blocking ridge~~

100 ~~over the Canadian Rockies and a slow-moving, cutoff, upper-level cyclonic circulation to its south over the western United States. Implicitly, all the studies mentioned~~ Implicitly, these studies and all the others available in the peer-reviewed literature point to the need for local and regional ~~quality high-quality~~ spatio-temporal rainfall data. Berne and Krajewski (2013) highlight the need to incorporate high-resolution weather radar information, even with some limitations, in flash flood hydrology.

105

~~Different authors have shown that antecedent soil moisture significantly influences the occurrence and behavior of flash floods. Rodriguez-Blanco et al. (2012) analyzed fifty-four flash flood episodes in Spain and determined that antecedent conditions are a vital point in runoff production. Castillo et al. (2003), using a modeling approach, highlighted the role of antecedent moisture conditions in flash flood~~

110 ~~occurrence associating them with different kinds of storm events. Aronica et al. (2012) used spatial and statistical analysis to reconstruct landslides and deposits, finding a connection between flash flood occurrence and soil moisture antecedent conditions. Tramblay et al. (2012) showed better flash flood model performance when using remotely sensed soil moisture data as initial conditions in a hydrological modeling study. Other authors have tried to understand the governing processes of flash~~

115 ~~floods from the geological formation of the basin (Adamovic et al., 2016; Vannier et al., 2016).~~

~~Due to the rapid nature of flash floods, they are more likely to occur in small and steep basins (Younis et al., 2008), highlighting the need for the availability of detailed temporal scale precipitation data (Norbiato et al., 2008) and high-resolution terrain information. Watersheds prone to these events are usually located in rural mountainous areas with poor gauge information (rain and level). The~~

120 ~~utilization of radar data to study flash flood generating storms is vital for understanding and forecasting these events (National Research Council 1996). One of the most critical challenges associated with flash floods is their simulation and prediction (Yamanaka and Ma, 2017; Borga et al., 2011; Marra et al., 2017). The fact that flash floods are more prone in small basins increases their intrinsic physical and measurement uncertainty (Wagener et al., 2007), difficulting their prediction (Hardy et al., 2016; Ruiz-Villanueva et al., 2013)~~

125 ~~. Many authors have assessed the influence of hills and stream slopes and evidence suggest the slopes of the hills are significantly more important for flash floods occurrence and magnitude than the stream slope (, eds.; Šálek et al., 2006; Roux et al., 2011; Yatheendradas et al., 2008).~~

~~Arguably one of the most meaningful applications of quantitative precipitation estimation (QPE) from a societal point of view is its use to improve flash flood forecasting. The use of weather~~

130 ~~radar QPE products in flash flood applications could potentially offset, in part, the lack of in-situ~~

4

precipitation products in small poorly gauged basins and become an important stepping stone for improving the state-of-the-art understanding of flash flood processes such as orographically enhanced extreme rainfall events and runoff generation (Creutin and Borga, 2003a). However, in some cases, there still exist limitations associated with the spatial resolution of radar retrievals (Šálek et al., 2006; Hardy et al., 2016). Nevertheless, several modern approaches involving radar information, in-situ precipitation data, model approximations and merging algorithms are promising (Braud et al., 2016).

The topography of Colombia is characterized by three branches of the Andes crossing the country south-to-north, generating a mixture of landscapes from high snow-capped mountains, vast highland plateaus, deep canyons to wide valleys, making some regions highly prone to flash flood occurrence. The likelihood of flash flood occurrence in Colombia is also high due to the spatio-temporal behavior of the Intertropical Convergence Zone, and the direction of the near-surface moist air flow leading to orographic enhancement of convective cores (Poveda et al., 2007). In the last decade, there have been several widespread and localized flash flood events in Colombia associated with climatological features and with the local intensification of rainfall events. The 2010-2011 La Niña event alone triggered 1233 flooding events and 778 mass removal processes in Colombia, with more than 3 million people affected and damages estimated by the "Comisión Económica para América Latina y el Caribe" in more than 6.5 billion US dollars. After this

After the 2010-2011 widespread disaster, several localized isolated events have occurred in the country with devastating consequences.

Between May 15th and May 18th, 2015, several storms took place over La Liboriana basin located in the municipality of Salgar, in the department of Antioquia (Colombia). By 2015, the population of Salgar was estimated at 17400 persons, 8800 residing in the urban area. La Liboriana is a small tropical basin(The present paper focuses on studying the processes triggering a flash flood in La Liboriana basin, a 56 km^2) km^2 basin located in the western range (Cordillera Occidental) of the Colombian Andes. During the night of May 17th, between 02:00 and 09:00 A.M. (local time), a precipitation event covered almost all the basin (hereafter referred to as event 1). Twenty hours later, between 23:00 P.M of, as a result of consecutive rainfall storms that took place between May 15th and May 17 and 02:00 A.M. of May 18 two successive extreme convective systems occurred over the basin with the maximum intensity in the upper hills (event 2). Event 1 corresponds mainly to a stratiform event, covering almost all the basin area and with an average precipitation accumulation of 47 mm. Event 2 accumulated, averaging over the basin, around 38 mm, however over the upper watershed the accumulation exceeded 180 mm. The occurrence of these successive rainfall events resulted in a flash flood that took 18th, 2015. The resulting flash flood dramatically affected the region, causing more than 100 human lives and affected casualties, affecting several buildings and critical infrastructure. The total investment for the reconstruction of Salgar´s infrastructure and the psychosocial attention of the community is, and resulting in a total reconstruction cost estimated

Figure 1. Example of infrastructure damage as a result of the La Liboriana May 18 of 2015 flash flood event. a) Aerial photograph before the event (2012) taken during a mission of the Department of Antioquia´s Government, and b) satellite image after the event (2015-05). The images show the destruction of most houses in that particular community, a bridge over La Liboriana, and the main road. The images also present changes in the delineation of the main channel as well as considerable erosion in the river margins.

at 36.000 million Colombian pesos (approximately 12,5 million dollars considering 2018 exchange rate), which corresponds to three times the annual income of the municipality. Figure 1 shows an example of infrastructure damage as a result of the flash flood event, and ~~satellite images~~ changes of the basin's main channel ~~before and~~ after the flash flood, showing considerable river ~~margins~~ margin and bed erosion. In spite of the data scarcity, including discharge measurements, the analysis of the successive rainfall events triggering the Salgar flash flood provide an interesting case of study for assessing the mechanisms depending on the soil moisture conditions and rainfall distribution.

La Liboriana basin flash flood is a typical case of prediction in ungauged basins ~~(PUB)~~ (Sivapalan et al., 2016; Seibert and Beven, 2009; Beven, 2007; Bonell et al., 2006; Yamanaka and Ma, 2017).

In this case, there are no local records of soils or land use and the local hydro-meteorological data is scarce or non-existent and certainly not available in real time. Due to the lack of data, La Liboriana case imposes a challenge for flash flood prediction and modeling. According to Blöschl et al. (2012), there are three methods for using models in ~~PUB~~ these cases. The first strategy is to obtain the required model parameters from historical basin behavior and the morphological characteristics of the basin. This strategy often leads to low model performance (Duan et al., 2006). The second approach is to inherit the hydrological calibration from a gauged neighboring watershed, which in this case does not exist. The third method is to parameterize the model based on proxy variables, such as hydraulic information obtained during field ~~recognition~~visits. In the case of the 2015 La Liboriana basin flash flood, there are no previous historical streamflow records, nor records from a neighboring watershed~~.~~

~~The present work aims to reconstruct the 2015 La Liboriana flash flood, not only to understand better the hydrological processes that took place during the event but also to serve as a proof of concept that hopefully leads to the development of a flash flood guidance low-cost tool based on the scarce information existent. Such a tool should be useful for decision-makers not only for short-term decisions in the context of an early warning system but also as a planning resource for long-term risk management. In particular, this work~~uses ~~-~~, thus we followed the third approach. In this work, we use precipitation information derived from radar~~QPE, satellite data~~, satellite and aereal images, and post-event field visits to reconstruct the Salgar flash flood event. ~~Also, this~~ This study addresses two broad hydrological issues. The first issue consists in exploring the relationship between rainfall spatio-temporal structure (Llasat et al., 2016; Fragoso et al., 2012), soil moisture and runoff generation (Penna et al., 2011; Tramblay et al., 2012; Garambois et al., 2013) during the successive rainfall events~~. The second issue consists~~, and the second issue in proposing a simplified ~~hydrological~~ hydrologic modeling scheme including land-slide and hydraulic sub-models to ~~detect and anticipate potential~~ assess the potential occurrence of flash flood events.

The methodology followed in this study makes use of a conceptual modeling framework that includes a ~~hydrological model~~ hydrologic model (Vélez, 2001; Francés et al., 2007a), a shallow landslide sub-model (Aristizábal et al., 2016), and a hydraulic sub-model ~~. The hydrological model, based on the work by Vélez (2001) and Francés et al. (2007a), simulates different hydrological processes as independent but interacting storages. The shallow landslide sub-model follows the formulation described in (Aristizábal et al., 2016). The hydraulic sub-model corresponds to a low-cost 1D model~~ (hereafter referred to as HydroFlash)~~that assumes infinite sediment supply and estimates the cross-sectional filled area at all time steps. The hydrological model includes the addition of ~~. The hydrologic model includes virtual tracers to explore separately the role of runoff and subsurface flow, as well as the relative importance of convective and stratiform precipitation in flash flood generation. The ~~convective and stratiform classification follows the methodology proposed by Houze et al. (2015)~~

7

215 ~~and Steiner et al. (1995). The~~ assessment of the interactions between runoff, subsurface flow, and convective-stratiform rainfall allows a better understanding of the short-term hydrological mechanisms leading to the flash flood event. ~~The model is parameterized using field information from a river cross-section located at the entrance of the urban area of Salgar.~~ A comparison between the results from both sub-models and the observed landslides scars and flooded spots helps to evaluate 220 the overall skill of the proposed methodology.

The document is structured as follows. Section 2 describes in more detail the region of study, La Liboriana basin, including geomorphological and climatological characteristics of the basin as well as the information sources used in this study. Section 3 presents a description of the overall methodol-225 ogy and the model used for the reconstruction of the 2015 La Liboriana flash flood event, including flow separation, shallow landslide parameterization, and the proposed hydraulic model. Section 4 describes the main results of the study, including model ~~parameterization and validation . Section 4 also~~ validation and sensitivity analysis, and presents results from the land-slide and inundation sub-models. Section 5 includes a discussion on the role of the rainfall structure in the flash flood 230 reconstruction~~and presents results from the land-slide and inundation sub-models~~. Finally, the conclusions are presented in section 6.

2 ~~Data and Area of~~ Study Site and Data

2.1 Catchment description

The urban area of Salgar municipality is located near the outlet of La Liboriana basin, a small (56 235 ~~km²~~km²) tropical watershed located in the westernmost range of Colombia's Andes (Figure 2). By 2015, the population of Salgar was estimated at 17400 persons, 8800 residing in the urban area. La Liboriana basin joins El Barroso river basin and both drain to Cauca river.

The availability of the ALOS-PALSAR Digital Elevation Model (DEM) (ASF, 2011), with a reso-240 lution of about 12.7 ~~m~~m, allows estimating the fundamental geomorphological features of the basin. The average slope of La Liboriana is 57.6 %, and the basin longitude and perimeter are 13.5 ~~km~~ km and 57.8 ~~km~~km, respectively. The Strahler-Horton order of the ~~principal~~ main stream is 5, and ~~the its~~ longitude and slope ~~of the principal stream~~ are 18.1 ~~km~~ km and 8.1 %, respectively. The highest elevation of the watershed (Cerro Plateado) reaches 3609 meters above sea level (m.a.s.l), while the 245 outlet of the basin is at 1316 m.a.s.l.. The ~~longitudinal profile (see Figure ??) exhibits considerable steepness in the upper basin. The~~ 99th slope percentile of order 1 streams is 78%. For streams order 2, 3, 4, and 5, the 99th slope percentile are 61, 27, 18 y 11%, respectively. Figure 2 shows the spatial distribution of the slopes in the watershed. These features are typical of Andean mountainous basins. ~~The hypsometric curve shows considerable elevation changes for a cumulative area below 33% (see~~

8

250 ~~blue line in Figure **??**).~~ Geomorphologically, this kind of watershed ~~is~~ tends to be prone to the occurrence of flash floods (Lehmann and Or, 2012; Penna et al., 2011; Martín-Vide and Llasat, 2018; Longoni et al., 2016; Ozturk et al., ?
.

~~Geographical context of Liboriana basin, located in Colombia, in the Department of Antioquia.~~
255 ~~The color bar represents the Height Above the Nearest Drainage (HAND). Low HAND values~~
~~correspond to areas prone to flooding.~~

At the sub-basin scale, La Liboriana exhibits a vast range of slopes and altitude differences. Figure 2 shows the Height Above the Nearest Drainage -HAND- model (Rennó et al., 2008) for La Liboriana. The HAND calculates the relative difference between cell i and its nearest streamflow cell j.
260 La Liboriana HAND exhibits values between 500 and 800 ~~m~~m. Near the outlet of the basin, over the banks, there are values close to 0 m. High HAND values at the upper region of the watershed often denote areas of high potential energy, with increased sediment production and frequent shallow ~~landslides~~ landslide occurrence. Banks with low HAND values are more susceptible to flooding and tend to correspond to areas prone to extensive damages caused by extreme events. While the
265 elevation differences described in Figure 2 are typical of the region, the social challenges lie in the high vulnerability of ~~the~~ Salgar given the location of the main urban settlement.

Vegetation and land use vary considerably within the basin. Figure 3 shows land use in different regions of the watershed from a 2012 aereal image. In the upper La Liboriana basin, there ~~are crop~~
270 ~~fields and tropical forests; a~~ is dense vegetation (see Zoom 1 in Figure 3), with a high percentage of tropical forests, with the presence of grass and few crop fields. A portion of the upper watershed is considered a national park. Hillslopes near the divide do not evidence significant anthropic intervention most likely due steepness of ~~the slopes in~~ this region. Down the hills and at the bottom of the valley there are coffee plantations (the primary economic activity of the region) and
275 pastures. Downstream (Figure 3, Zoom 2), it is evident the presence of crops among forest and grass. Near the middle of the basin (Figure 3, Zoom 3), the presence of crops is more notorious and human settlements and roads start to appear. The watershed exhibits grazing areas and urban development near the river banks. In Figure 3, Zoom 4, corresponding to the first affected urban area from upstream to downstream during the flash flood, it is also possible to see a marked presence of
280 crops and some forest patches. Finally, zoom 5 shows the main urban area of Salgar surrounded by crops, grass and an important loss of forest coverage.

~~The Andean Colombian region tends to present well-developed soils of different textures with a~~
~~predominance of limes and clays.~~
285 One of the challenges for hydrological modeling and risk management in the country is that soils are not well mapped; the national soil cartography is usually available in a 1:400.000 scale. At this
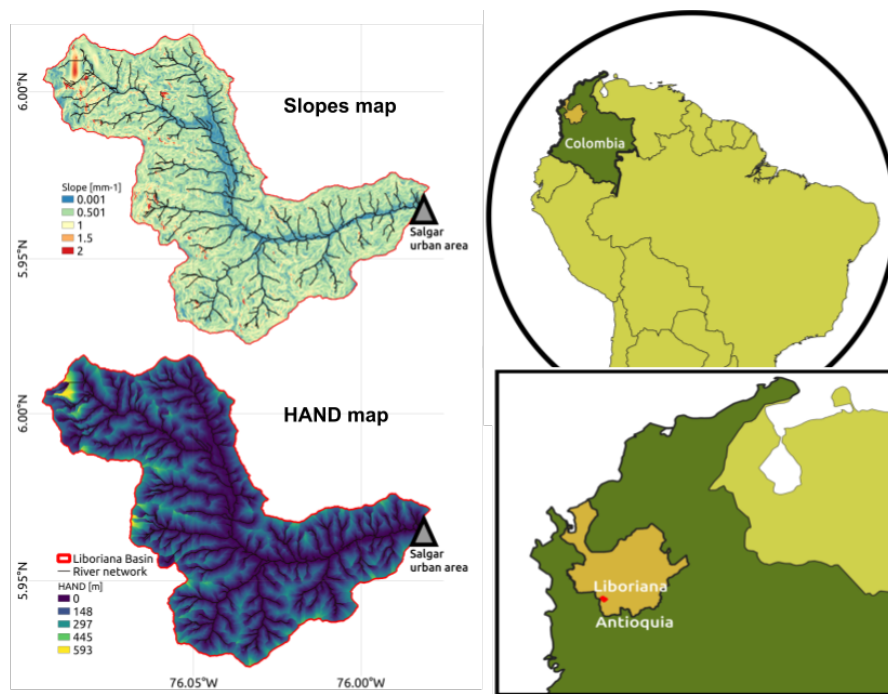
9

Figure 2. ~~Longitudinal profile~~ Geographical context of Liboriana basin, located in Colombia, in the ~~principal stream (colored line) from the upper part~~ Department of Antioquia. The color bar represents the ~~basin to its outlet at~~ Height Above the ~~entrance of~~ Nearest Drainage (HAND). HAND values where estimated using the ~~urban area, hypsometric curve~~ same resolution of the ~~drainage basin~~ DEM (~~blue line~~12.7 m). Low HAND values correspond to areas prone to flooding.

scale, the municipality of Salgar, including La Liboriana basin, corresponds to only one category of soil texture. ~~The only available information corresponds to descriptions by regional authorities. Osorio (2008)describe~~ Osorio (2008), based on field campaign observations and laboratory tests, described La Liboriana soils as a well-drained soil with poor retention capacity. Organic material is predominant in the first layer and clay loam soil within the second one. The depth of the soil is hillslope dependent, varying ~~between~~ from 20cm ~~and~~ to 1m (Osorio, 2008). Table 1 provides a summary of soil characteristics for five different categories, all as a function of slope. Each soil category has a corresponding depth and a qualitative description of permeability and retention.

~~A field campaign~~

2.2 Flash flood post-event observations

We conducted a field campaign a few days after the May 18th flash flood event ~~was instrumental in obtaining~~ to assess cross-section geometry along the main channel in different sites, including at the outlet of the basin. ~~The~~ Unfortunately, most of the affected areas were not accessible after the event
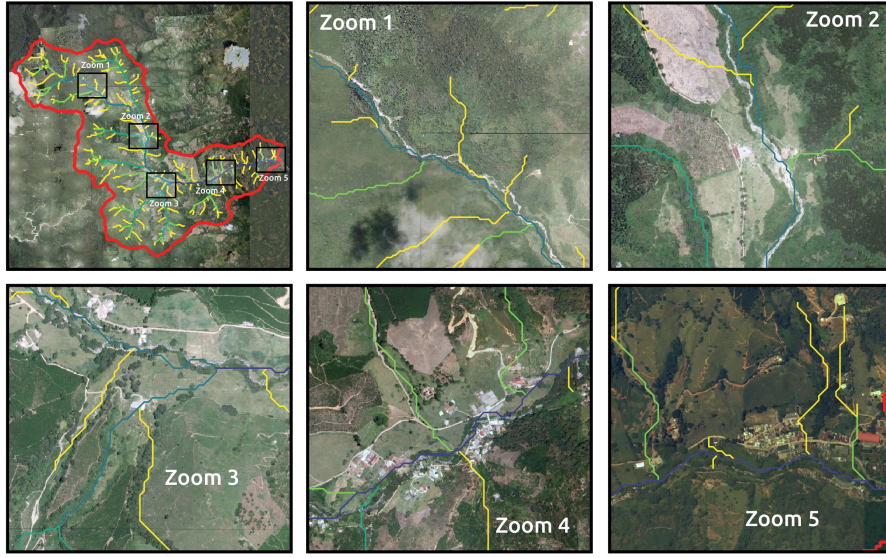
Figure 3. Land use in different regions of La Liboriana watershed from a 2012 aereal images (Source: Department of Antioquia.

Table 1. Description of the soils in the region (Osorio, 2008).

Type	Slope	Depth [m]	Retention	Permeability
Class III	12-25	0.6	Mean	Mean
Class IV	<12	0.6	Low	High
Class VI	25-30	1.0	Mean	Mean
Class VII	30-50	0.3	Too Low	Slow
Class VIII	>50	0.2	Too Low	Slow

and it was not possible to obtain reliable information in other locations along the main channel other than at the outlet of the basin. During the campaign, we measured sectional distances and surface water speeds at different points of the streamflow. We also identified traditional post-event terrain, land-cover, vegetation and infrastructure markers to assess the high-water marks associated with the

305   peak of the flash flood. Figure 4 presents the selected cross-section used for the estimation of the maximum discharge during the flash flood given its geometrical and hydraulic regularity. The section has a rectangular shape, ~~and it is~~ 4.6 ~~m wide and has~~ m wide and a height of 5 ~~m~~ m for a total area of about 23 ~~m^2~~ m^2. A visual inspection of the flooded ~~infrastructure around this section~~ house around the section, located 4-5 m away from the channel, reveals the presence of mud marks on the walls

310   with heights varying between 0.5 and 1.2 ~~m. These mud stains are evident in buildings located 4-5 m away from the channel~~ m (see Figure 4). The area of the section plus the flooded area during the

11

Figure 4. Channel cross-section shown an example of flooded infrastructure after the flash flood event. The section shows mud marks on the walls with heights varying between 0.5 and 1.2 ~~m~~m. These mud stains are evident in buildings located 4-5 ~~m~~ m away from the channel. The photograph also shows the width of the channel and the total estimated depth during the flash flood.

event was estimated to be approximately 37 ~~m^2. Assuming flow speeds~~ m^2. During the campaign we measured surface speeds in the channel oscillating between 2 and 3 ms^{-1}. In instrumented basins in the region, with similar characteristics in terms of area and slopes, we have recorded peak flow surface water speeds oscillating between 5 and ~~6 m/s, the total discharge required to generate~~ 7 ms^{-1}. By assuming an area of 37 m^2 and the mentioned surface speeds, we estimate that the observed flash flood ~~vary~~ peak flow may have been between 185 and 222 ~~m^3/s. In this work, the soil information and the field campaign are used to parametrize a hydrological model~~m^{3}s^{-1}. The timing of the peak flow is also important information. Local authorities reported that the peak streamflow reached the urban perimeter after 2:10 a.m. on May 18th. Some reports state that the peak flow in the most affected community occurred around 2:40 a.m.

There is also relevant aerial information before and after the occurrence of the event. During 2012, the Department of Antioquia conducted a detailed aerial survey of the Salgar municipality, and few days after the event Google displayed publically high detailed satellite images of the same region. The contrast between both products provides information about flooded areas and landslide locations. Field campaign estimates and ~~satellite~~ aerial imagery are central to validate the results obtained from the proposed ~~hydrological model~~models.

~~The reconstruction~~

2.3 Rainfall Information

The assessment of the 2015 Salgar flash flood event following a hydrological modeling strategy uses a radar-based QPE technique developed by Sepúlveda and Hoyos (~~2018)~~2019) using rainfall

gauges and disdrometers within the radar domain to obtain spatiotemporal precipitation maps over
the basin. A detailed description of the rainfall estimation, as well as the overall meteorological
conditions that led to the La Liboriana extreme event, are described in a companion paper (Hoyos
et al. ~~2018~~2019). The QPE technique uses retrievals from a C-band polarimetric Doppler weather
radar operated by the Sistema de ~~Alertas Tempranas~~ Alerta Temprana de Medellín y ~~del~~ el Valle de
Aburra (SIATA, ~~is~~ a local early warning system from a neighboring region, www.siata.gov.co)~~and it~~
~~is located at 100km~~, located around 90 km away from the basin. The radar has an optimal optimum
range of 120 ~~km radius~~ km radius for rainfall estimation and a maximum operational range of 240
~~km~~km for weather detection. The radar operating strategy allows obtaining precipitation informa-
tion every 5 ~~min and the~~minutes with a spatial resolution is about 128 ~~m. The sensor is a C-band~~
~~polarimetric Doppler weather radar operated by the Sistema de Alertas Tempranas de Medellín y~~
~~del Valle de Aburra (SIATA, a local early warning system from a neighboring region, www.siata.~~
~~gov.co)~~m. The results of the radar QPE methodology indicate that the rainfall estimation works well
within a radius of 120km. Despite the distance between the radar and the basin, and the mountains
between them, there are no blind spots for the radar. A comparison between the radar QPE estimates
and records from two rain gauges installed three days after the flash flood event show a correlation for
an hourly time scale of 0.65. In addition to the rainfall quantification, radar retrievals, before feeding
the hydrologic model, are classified in convective and stratiform areas following a methodology
proposed by Houze et al. (2015) and Steiner et al. (1995).

Between May 15th and May 18th, 2015, several storms took place over La Liboriana basin. During
the night of May 17th, between 02:00 and ~~located at 100km away from the basin~~09:00 a.m. (local
time), a precipitation event covered almost all the basin (hereafter referred to as precipitation Event
1). Twenty hours later, between 23:00 p.m. of May 17 and 02:00 a.m. of May 18 two successive
extreme convective systems occurred over the basin with the maximum intensity in the upper hills
(precipitation Event 2). Event 1 corresponds mainly to a stratiform event, covering almost all the
basin area and with an average precipitation accumulation of 47 mm. Event 2 accumulated, in
average over the basin, around 38 mm, however over the upper watershed the accumulation exceeded
180 mm. Figure 5a presents the temporal evolution of the convective-stratiform rainfall partitioning
during both Events 1 and 2. The main difference between both events is the timing of the convective
versus stratiform participation within each case. Event 1 started as a stratiform precipitation event
moving from the southwest, from the Department of Chocó to the Department of Antioquia across
westernmost Andes mountain range. ~~The radar has an optimal optimum rangeof 120 km radius and~~
~~a maximum operational range of 240 km. The radar operating strategy allows obtaining precipitation~~
~~information every 5min and with a spatial resolution is about 128 m~~Chochó is the rainiest department
in Colombia, and one of the wettest places on Earth, due to the inflow of moisture from the Pacific
Ocean and the orientation of the Andes mountain range (Poveda and Mesa, 2000; Mapes et al., 2003)

. After 3 hours of stratiform rainfall, training convective cores move over La Liboriana basin generating intense precipitation peaks during 2.5 hours. It is important to note that these cores did not strengthen within La Liboriana basin; these systems formed and intensified over the western hills of Farallones de Citará draining to the Department of Chocó towards the Atrato river. The latter is not a minor fact

375   because once the convective system moved with a northeast direction, the maximum intensity cores did not fall over the steepest hills of La Liboriana basin but rather near the basin outlet where the slopes are considerably flatter. Figure 5b shows the spatial distribution cumulative rainfall during Event 1, with the maximum precipitation located towards the bottom third of the basin. Event 2, on the other hand, started as a thunderstorm training event with two convective cores moving from

380   the southeast followed by remaining stratiform precipitation. Even though the average cumulative rainfall over the basin was 9 mm less than during Event 1, this event is characterized by orographic intensification within the basin leading to a more heterogeneous spatial distribution and with the highest cumulative precipitation in the steepest portion of the basin (see Figure 5b). Event 2 spatial distribution and highly localized observed intensities most likely led to the flash-flooding episode,

385   as it is explored in this work.

3   ~~Methodology~~

The data requirements, and rainfall preprocessing needed for the overall methodology followed in the reconstruction of the 2015 Salgar flash flood ~~, is presented in an illustrative~~ are summarized in

390   Table 2 and are presented in a schematic diagram in Figure 6.

3   Methodology

3.1   Hydrological modeling framework

The availability of radar-based QPE and a detailed DEM allows the use of a modeling framework

395   based on the distributed ~~hydrological~~ hydrologic model described in Vélez (2001) and Francés et al. (2007a) with important modifications ~~(left column in Figure 6). The hydrological~~. The hydrologic model simulates different hydrological processes as independent, but interacting storages (second row, left panel in Figure 6). The model distributes processes by cells; in each cell, five tanks represent the hydrological processes including capillary (tank 1), gravitational (tank 2), runoff (tank 3),

400   baseflow (tank 4) and channel storage (tank 5). The state of each tank varies in function of vertical and lateral flows as shown in the diagram, where the storage is represented by S_i, the vertical input to each tank by D_i, which in turns depends on the vertical flow through tanks R_i. E_i represents the downstream connection between cells, except for tank 1, where E_1 represents the evaporation rate.
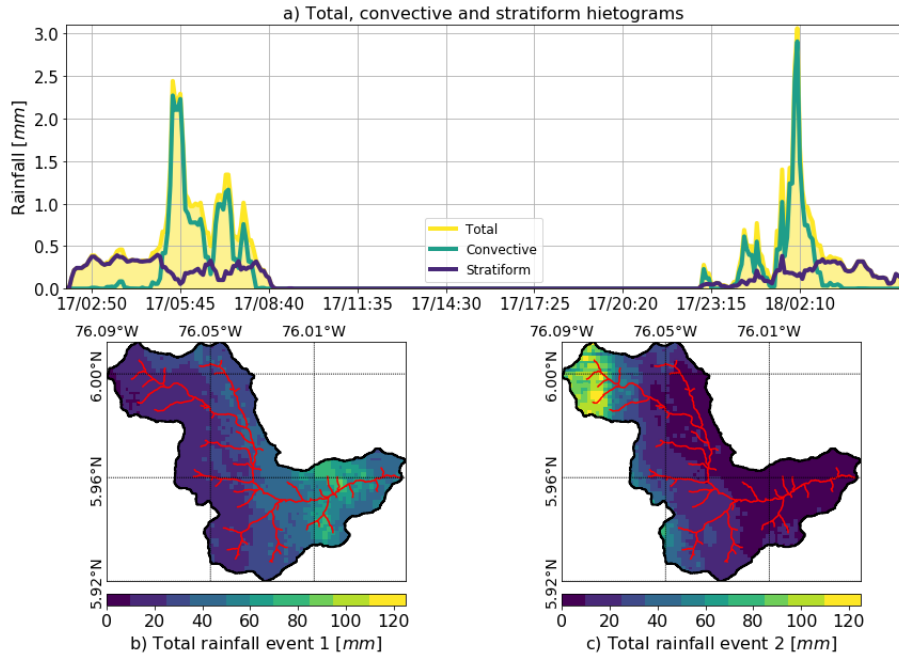
14

Figure 5. a) Temporal evolution of the convective-stratiform rainfall partitioning during both Events 1 and 2. The figure shows the total rainfall (yellow), and the convective (blue) and stratiform (green) portions integrated over La Liboriana basin. b) and c) Spatial distribution of the cumulative rainfall during Events 1 and 2 over La Liboriana basin.

Vertical flows are only time dependent, while lateral flows could also depend on the actual state of
405   the tank (kinematic approximation).

~~Illustrative diagram of the methodology followed in the present study. The left column represents the availability of radar-based QPE and a detailed DEM as the basis of the modeling framework and the mains aspects of the distributed hydrological model used. In each cell five tanks represent the~~
410   ~~hydrological processes including capillary (tank 1), gravitational (tank 2), runoff (tank 3), baseflow (tank 4) and channel storage (tank 5). The state of each tank varies in function of vertical and lateral flows as shown in the diagram, where the storage is represented by S_i, the vertical input by D_i which in turns depends on R_i. E_i represents the downstream connection between cells, and evaporation. The implementation of convective and stratiform rainfall separation and virtual tracers are presented~~
415   ~~in the top two right panels. The implementation of the shallow landslides model and HydroFlash are schematized in the bottom two right panels.~~

The model modifications fall in four different categories: (i) the direct use of radar QPE as a source of rainfall information, (ii) the implementation of virtual tracers for surface and subsurface discharge as well as for convective and stratiform water tracing, (iii) the ~~development of~~
420   ~~two modules for hazard assessment, and (iv) the~~ enforcement of a maximum gravitational stor-

15

Item	Description	Period	Usage
Radar data	QPE rainfall estimations	2015-05-17 to 2015-05-18	Hydrologic model runs. Rainfall characterization and event analysis.
Field campaign	Maximum streamflow estimation trough visual inspection	2015-05-20	Hydrologic model comparison for indirect validation.
Satellite imagery	Visible channel compositions from the Digital Globe CNES imagery	2015-05 (post-event)	Flash flood model validation, shallow land-slides model validation, and comparison with pre-event conditions.
Aerial photos	Aerial photos taken by the government of Antioquia during 2012.	2012	Pre-event conditions comparison.
Soils description	Physical description of the soils of the region by Osorio (2008)	2008	Hydrologic model setup.

Table 2. Summary of the data used for the model setup.

age (H_g) to allow Hortonian runoff (return flow from S_3 (tank 3) to S_2 ~~). The virtual tracers are critical to explore separately the relative role of superficial runoff and subsurface flow, as well as the relative importance of convective and stratiform precipitation in flash flood generation. The convective and stratiform classification follows the methodology proposed by Houze et al. (2015)~~

425 ~~and Steiner et al. (1995)~~(tank 2)), and (iv) the development of two modules for hazard assessment. The implementation of ~~convective and stratiform rainfall separation and virtual tracers are presented~~ virtual tracers is represented in the top two right panels of the ~~illustrative~~ diagram in Figure6.~~The hydrological modelallows hazard assessment by coupling a shallow landslide model(Aristizábal et al., 2016)~~

~~.~~

430

3.1.1 Hydrological runoff scheme modification

In the model, horizontal flow equations could be either linear or potential, as shown in equation 1. In the modified hydrologic model, β and α are estimated by the user and then set into the model. In the non-lineal approximation β is a coefficient that summarizes local properties invariant over time, 435 like the slope or the hydraulic conductivity. α is an exponent that change in function of the adopted
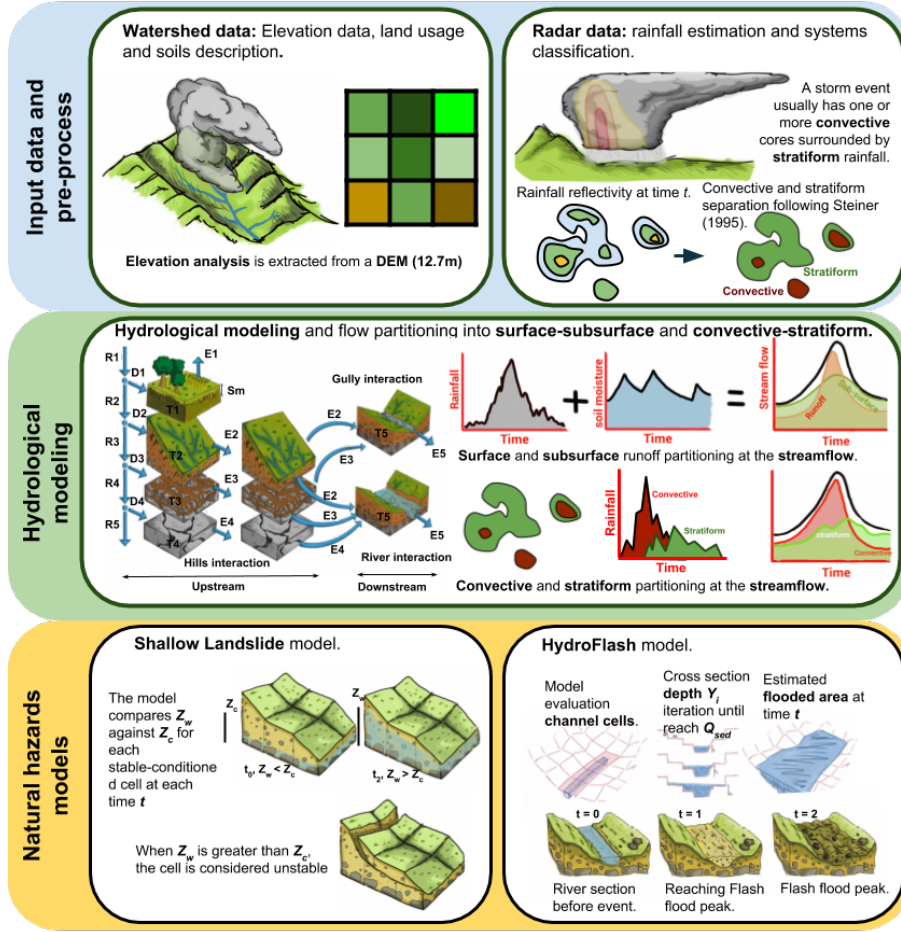
16

Figure 6. Illustrative diagram of the methodology followed in the present study. The top row represents the availability of a detailed DEM and radar-based QPE as the basis of the modeling framework. The second row represents the mains aspects of the distributed hydrologic model used. In each cell five tanks represent the hydrological processes including capillary (tank 1), gravitational (tank 2), runoff (tank 3), baseflow (tank 4) and channel storage (tank 5). The state of each tank varies in function of vertical and lateral flows as shown in the diagram, where the storage is represented by S_i, the vertical input by D_i which in turns depends on the vertical flow through tanks R_i. E_i represents the downstream connection between cells, and evaporation. The implementation of convective and stratiform rainfall separation and virtual tracers is also portrayed. The implementation of the shallow landslides model and HydroFlash are schematized in the bottom row.

approximation. From equations 1 to 3, $A_i(t)$ corresponds to the sectional area of each storage, $A_i(t)$ vary in function of the tank storage $S_i(t)$ according to equation 4.

$$v_{tank}(t) = \beta A_i(t)^\alpha \tag{1}$$

17

Non-linear equations in lateral flows could result in a better representation of processes at high
440 resolutions (Beven, 1981; Kirkby and Chorley, 1967). A non-linear approximation to runoff is presented
in equation 2. This approximation is a modification of Manning's formula for flow in gullies. According
to Foster G.R. (1984), ε and ~~a new low-cost 1d hydraulic flash flood model referred to here as~~
~~**HydroFlash**. The implementation of~~ e_1 are a coefficient and an exponent used to translate the
manning channel concept into multiple small channels or gullies. The values of ε and e_1 are 0.5
445 and 0.64, respectively (Foster G.R., 1984). A_2 is the corresponding sectional area obtained from S_2
by using the equation (4). And S_0 is the slope of the cell.

The non-linear equation 3 corresponds to an adaptation of Kubota and Sivapalan (1995) formula
for subsurface runoff where k_s is the saturated hydraulic conductivity, and the exponent b is dependent
on the soil type, assumed equal to 2. A_g is the equivalent cross-section area to the maximum
450 gravitational storage (H_g). A_3 is the corresponding sectional area of the gravitational storage (S_3)
obtained by using equation (4). There is also return flow from tank 3 to tank 2 when $S_3 = H_g$,
representing runoff generation by saturation.

$$v_2 = \frac{\varepsilon}{n} S_0^{1/2} A_2(t)^{(2/3)e_1} \tag{2}$$

455
$$v_3 = \frac{K_s S_o^2}{(b+1)A_g^b} A_3(t)^b \tag{3}$$

The equations describe the momentum of a kinematic wave approximation. In both cases, velocity
depends on the tank storage. These relations are summarized in equation 1, that could be solved
numerically coupled with a mass balance equation (equation 4). This equation takes into account
the storage at each time step ($S_{tank}(t)$), the longitude of the element (Δx), the time step size (Δt),
460 and the speed estimated for the flow in the time step ($v_{tank}(t)$). Equation 4 is related to equation 1
through the velocity term for that tank (v_{tank}) and the ~~shallow landslides model and HydroFlash are~~
~~schematized in the bottom two right panels of the illustrative diagram in Figure 6.~~ cross-sectional
area of the tank (A_{tank}). The solution to v_{tank} and A_{tank} is obtained through an iterative scheme.
The total outflow from the tank is calculated using equation 5.

465 ~~For the technically inclined reader, the hydrological model and sub-models are written in Fortran~~
~~90, and the interface to the model, pre-process, and post-process tools are in python 2.7. The Fortran~~
~~code is warped to python using **f2py** (Peterson, 2009) and it is publicly available under the Watershed~~
~~Modelling Framework **WMF** in a web repository ().~~

$$A_i(t) = \frac{S_{tank}(t)}{\Delta x + v_{tank}(t)\Delta t} \tag{4}$$

470

$$E_{tank}(t) = A_{tank}(t)v_{tank}(t)\Delta t \tag{5}$$

3.2 ~~Virtual Tracers~~

3.1.1 Virtual Tracers

Virtual tracers are implemented into the model to discriminate streamflow source in superficial runoff
and subsurface flow and to assess the portion of streamflow from convective rainfall and stratiform
precipitation, recording at each time stem and each cell the source of water. The model archives the
results of the virtual tracing algorithm at the outlet of the basin and at each reach allowing the study
of the role of flows from different nature during extreme events at different spatial scales to get more
insights about the soil-driven flow regulation. ~~The soil texture and composition could play diverging
roles during extreme events. The soil could work as a porous medium in which the water travels fast,
making the subsurface flow an essential part of the hydrograph, or on the other hand, its saturation
could lead to a decrease in infiltration rates and a potential increase of surface runoff generation.~~

The flow separation module operates in tanks 2 (runoff storage) and 3 (subsurface storage). The
module marks water once it reaches any of those two tanks and the runoff-subsurface flow percent-
age are taken into account once the water enters tank 5 (the channel). At this point, the scheme
assumes that the water in the channel is well mixed, implying that the flow percentage is constant
until a new inflow enters the channel.

~~Both spatial and temporal rainfall variability influence the hydrograph Shope (2016). Stratiform
rain cells cover large areas and are related to long duration hydrographs with low peak flow. On the
other hand, convective rainfall cells cover limited areas and are related to short duration hydrographs
with high peak flows. Stratiform rainfall tends to recharge the basin, while convective tends to
increase runoff generation and the formation of the hydrograph. In the literature, these associations
have often been more qualitative than quantitative (Creutin and Borga, 2003b; Šálek et al., 2006; Borga et al., 2014)
.~~

~~Rainfall from radar reflectivity fields is classified into stratiform and convective using the Steiner et al. (1995)
approach before the implementation of the rainfalltracer. At~~ With a similar concept, the model also
follows convective and stratiform rainfall. For this, at each time step, the model takes into account
the ~~total rainfall , assuming~~ rainfall classified as convective or stratiform, and assumes that at each
particular cell the precipitation is either entirely convective or entirely stratiform. This assumption
could lead to estimation errors at basins represented by coarse cells (low DEM resolution) where
convective and stratiform precipitation are likely to coexist. In the present study the spatial reso-
lution of the DEM is $12.7m$, higher than the resolution of the radar retrievals (about $125m$), so
the potential convective and stratiform rainfall concurrence is very low, and it could not be identi-
fied using the Steiner et al. (1995) approach.~~Once within the model, rainfall separation follows the~~

~~methodology proposed for flow type separation.~~

3.2 ~~Hazards Assessment~~

510 ### 3.1.1 Hydrologic model calibration

~~During the 2015 La Liboriana flash flood event, two central processes took place. Shallow landslides occurred in the upper basin , and a flash flood generated flooding, and human and infrastructure losses.~~ The hydrologic model requires a total of ten parameters. Table 3 includes all the parameters used in the model. The values of the parameters were derived from the soil properties described in

515 section 2. Due to the lack of detailed information in the region, parameters such as the infiltration and percolation rates are assumed as constant in all the basin. Other parameters such as the capillary and gravitational storage vary in function of geomorphological characteristics of the basin such as the elevation and slope. According to Francés et al. (2007b), during the calibration process, each physical parameter is scaled by a constant value in the entire basin. Table 3 includes the mean value

520 for all the parameters used in the model and the scalar value adjusted during the model calibration.

~~Shallow landslides sub-model~~

3.2 Shallow landslides sub-model

The shallow landslides submodel coupled to the ~~hydrological~~ hydrologic model is proposed by Aristizábal et al.. The ~~model conceptualizes the stability of a cell based on the concept of an infinite~~

525 ~~slope described by the geomorphological and soil properties of the cell. The model~~ submodel classifies cells into three groups: unconditionally stable, conditionally stable and unconditionally unstable. Figure 7 describes the variables of the model and the balance of forces considered. Three parameters determine stability of each cell: (i) residual soil thickness water table $Z_{i,min}$ estimated as in equation ~~(6)~~6, (ii) the maximum soil depth at which a particular soil remains stable $Z_{i,max}$ estimated as

530 in equation ~~(7)~~7, and (iii) the maximum slope at which the soil remains stable $\beta_{i,0}$ estimated as in equation ~~(8).~~

~~The geotechnical conceptual model~~8. In the equations and in the Figure 7 γ ~~is the soil bulk density, is the soil bulk density,~~ γ_w ~~is the water density, is the water density,~~ Z_w ~~is the saturated soil thickness above the slip surface, is the saturated soil thickness above the slip surface,~~ Z ~~is the soil thickness~~

535 ~~measured vertically, is the soil thickness measured vertically,~~ β ~~is the gradient of the hillslope. And is the gradient of the hillslope, and~~ ϕ ~~is the soil stability angle.~~ Q_L and Q_R ~~are the resultant forces on the sides of the slice~~are the resultant forces on the sides of the slice.

$$Z_{i,min} = \frac{C'}{\gamma_w cos^2\beta tan\phi + \gamma cos^2\beta(tan\beta - tan\phi)} \tag{6}$$

20

Parameter Name	Symbol	Scalar Parameter	Mean Value	Spatial distribution
Capilary storge	Hu [mm]	1	39	In function of the slope
Gravitational storage	Hg [mm]	1	34	As a function of the slope
Evaporation rate	Etr [mm/s]	0.1	0.01	As a function of the DEM
Infiltration rate	ks [mm/s]	2.7	0.0012	Lumped
Percolation rate	kp [mm/s]	0.8	0.00012	Lumped
System losess	Kf [mm/s]	0	0.0	Lumped
Surface speed	vr [m/s]	0.5	6.4	As a function of the slope and storage
Subsurface speed	vs [m/s]	1	7.1	As a function of the slope, Hg and storage
Subterranean speed	vb [m/s]	0.5	0.000095	Lumped
Channel speed	vc [m/s]	1	0.95	As a function of the slope, acumulated area, and storage

Table 3. Hydrologic model parameters.
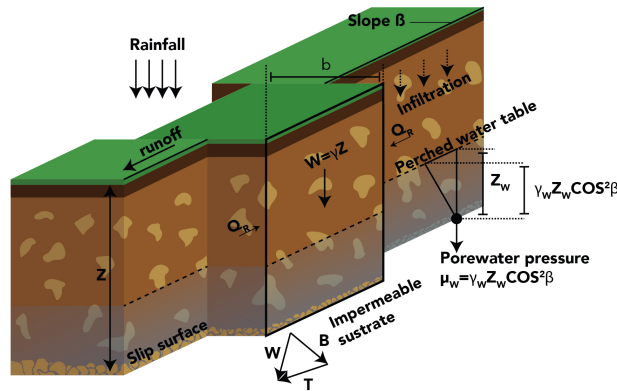
Figure 7. The geotechnical conceptual model. Figure and description are adapted from Aristizábal et al. (2016).

$$Z_{i,max} = \frac{C'}{\gamma cos^2 \beta (tan\beta - tan\phi)} \tag{7}$$

$$\beta_{i,0} = tan^{-1}\left[tan\phi\left(1 - \frac{\gamma_w}{\gamma}\right)\right] \tag{8}$$

The model assess conditionally stable cells in function of their perched water table for each cell ($Z_{i,w}$, equation ~~(9)~~ 9) and the critical satured depth ($Z_{i,c}$, equation (10)). Slope failure occurs when $Z_{i,w}$ is greater than $Z_{i,c}$. ~~$Z_{i,c}$ is obtain using equation (10) .~~

$$Z_{i,w}(t) = \frac{S_{3,t}}{W_c - W_{fc}}$$

$$Z_{i,c} = \frac{\gamma}{\gamma_w} Z \left(1 - \frac{tan\beta}{tan\phi}\right) + \frac{C'}{\gamma_w cos^2 \beta tan\phi}$$

~~where~~ At equation (9) $S_{3,i}$ represents gravitational storage, Ws and W_{fc} the soil saturation and field capacity respectively~~, γ represents soil density, ϕ is the soil stability angle, ~~. And in equation (10) C' represents the soil cohesion and β the cell slope.

~~**Flash flood submodel (HydroFlash)**~~

$$Z_{i,w}(t) = \frac{S_{3,t}}{W_c - W_{fc}} \tag{9}$$

$$Z_{i,c} = \frac{\gamma}{\gamma_w} Z \left(1 - \frac{tan\beta}{tan\phi}\right) + \frac{C'}{\gamma_w cos^2 \beta tan\phi} \tag{10}$$

3.3 Flash flood submodel (HydroFlash)

~~It is common to use complex hydraulic 2D and 3D models, such as Iber (Cea and Blade, 2015) or HEC (Gibson et al., 2010) for flood spots identification. This kind of modeling requires detailed information about the terrain and river bathymetry and are usually implemented for a particular river cross section due to the high information demand and high computational costs, precluding the operational implementation of 2D and 3D methodologies in regions with scarce resources. Also, this traditional hydraulic methodology tends to analyze only some network elements, overlooking the complexity of the basin.~~ In this work, we introduce a low-cost 1D hydraulic model for flash flood simulation referred to as HydroFlash. The model extracts the cross-profile from the DEM for each cell considered part of the network, estimating flood spots at each network cell during execution time.

The model requires hydraulic parameters for all network cells to determine flash-flooding spots. Channel width is estimated using the Leopold (1953) approach $W_i = 3.26\overline{Q_i}^{0.469}$. Channel slope $(S_{i,0})$ is obtained as the mean value of the slopes that correspond to the cells of a hydrological reach.

570   The characteristic particle diameter $D_{i,50}$ is assumed equal to 0.138~~and constant~~m and constant (Golden and Springer, 2006). The cross-section (C_s) is obtained from the DEM, for every network cell, perpendicular to the flow direction of the cell (~~$D_{i,8}$~~$D8_i$).

For each time step t and for each stream cell, equation ~~(11)~~11 determines the height of the wa-

575   ter table $Y_i(t)$ using the simulated streamflow ~~$Q_{i,sim}(t)$~~$Q_{i,sim}(t)$ and flow velocity $v_{i,sim}(t)$. The model calculates the friction velocity (~~$v_{fr,i}$) using Y_i~~$v_{fr,i}(t)$) using $Y_i(t)$ as in equation (12) derived from Keulegan and Rouse equations ~~(Takahashi, 1991). Equations (13) and (14)~~(Takahashi, 1991; Savage and Sayed, 1984). Equations 13 and 14 allow the estimation of the concentration ($c_i(t)$) and constitutive coefficients (~~r_i~~$r_i(t)$), respectively. In equation 13 C_{max} represents the maximum sediment concentration;

580   according to Obrien (1988) C_{max} is near 0.75 during flash floods. The stream flow plus estimated sediments and rubble is estimated according to equation ~~(15)~~15.

$$Y_i(t) = \frac{Q_{i,sim}}{v_{i,sim}w_i}\, \frac{Q_{i,sim}(t)}{v_{i,sim}(t)w_i} \tag{11}$$

$$v_{fr,i}(t) = \frac{v_{i,sim}}{5.75\,log\left(\frac{Y_i}{D_{i,50}}\right)+6.25}\, \frac{v_{i,sim}(t)}{5.75\,log\left(\frac{Y_i(t)}{D_{i,50}}\right)+6.25} \tag{12}$$

585

$$c_i(t) = C_{max}\left(0.06\,Y_i(t)^{\frac{0.2}{v_{fr,i}}}\right)^{\frac{0.2}{v_{fr,i}(t)}} \tag{13}$$

$$r_i(t) = \frac{1}{D_{i,50}}\left[\frac{g}{0.0128}\left(\frac{9.81}{0.0128}(c_i+(1-c_i)\frac{\gamma_w}{\gamma_{sed}}\,\frac{\gamma_w}{\gamma_{sed}})\right)\right]^{1/2}\left[\left(\frac{C_{max}}{c_i}\,^{(1/3)-1.0}\right)^{1/3}-1\right] \tag{14}$$

590    $$Q_{i,sed}(t) = Q_{i,sim}\frac{1+c_i}{1-c_i}\, \frac{Q_{i,sim}(t)}{1-c_i(t)} \tag{15}$$

~~assuming~~Assuming infinite sediment and rubble supply, ~~$Q_{i,sed}$~~$Q_{i,sed}(t)$ is the maximum stream flow for the section. To determine the flooded area, ~~an equivalent $Y_{i,sed}$~~a flood depth $F_{d,i}(t)$ must be found in order to obtain an stream flow ($\hat{Q}_{i,sed}$$\hat{Q}_{i,sed(t)}$) (equation ~~(18)) that equals $Q_{i,sed}$. The estimation of $Y_{i,sed}$ is an iterative process. The model obtains the~~18) that equals $Q_{i,sed}(t)$. The

595 search of $F_{d,i}$ is done iteratively by making small increments to it. Both flooded area ($A_{i,sed}$) based on $Y_{i,sed}$ and equation (17) $A_{i,sed}(t)$) and flooded section ($F_{f,i}$) are obtained in the process. At each iteration, $F_{d,i}$ is an estimated depth (equation 16), measured from the bottom of the section (b_i) to a guess elevation of the section ($\Delta y \cdot j$). The depth of $F_{d,i}$ increases with each iteration as j takes values between 1 and the total number of iterations with a step of 1. At the end of each iteration,

600 $A_{i,sed}(t)$ is estimated with equation 17, in which $F_{sec,i}$ corresponds to the section i extracted from the DEM. Based on the value obtained for $A_{i,sed}(t)$, the model estimates $\hat{Q}_{i,sed}$ (equation 18). The process stops when $\hat{Q}_{i,sed}$ is similar to $Q_{i,sed}$, at this point, the flooded section $F_{f,i}$ corresponds to the values of $F_{sec,i}$ that are below $F_{d,i}$.

$$_{i,sed}F_{d,i} = \frac{2}{5} r b_i (j + \Delta y_{i,sed})^{\frac{3}{2}} S_{i,0} 0.5_{i,sed} \cdot j \tag{16}$$

$$605 \quad \hat{A}_{i,sed} = \Delta x \sum_{j=1}^{N} (Y_{i,sed} + \Delta y_{i,sed}) F_{d,i} - C_{j,s} F_{sec,i} \tag{17}$$

$$\hat{Q}_{i,sed}(t) = \left(\frac{2}{5}\right) r_i(t) (j\Delta y)^{\frac{3}{2}} S_{0,i} \hat{A}_{i,sed}(t) \cdot 0.5 \tag{18}$$

Resulting flood maps might evidence the presence of small isolated flood spots and discontinuities at flood spots where flow direction changes from orthogonal to diagonal or vice-versa. We included two post-processing steps to correct these issues by (i) using an image processing erosion algorithm

610 (Serra, 1983) to remove the small isolated flood spots. The erosion is performed once with a 3x3 kernel, and (ii) to solve the flow direction discontinuities, each flooded cell seeks to flood its eight neighboring cells. A neighbor cell is also flooded if the altitude of the original flooded cell plus the flood depth is higher than its altitude.

3.4 Hydrological runoff scheme modification

615 Horizontal flow equations could be either linear or potential, as shown in equation (1). In the modified hydrological model, β and α are estimated by the user and then set into the model.

$$v_{tank}(t) = \beta A(t)^{\alpha}$$

Non-linear equations in lateral flows could result in a better representation of processes at high resolutions (Beven, 1981; Kirkby and Chorley, 1967). A non-linear approximation to runoff is presented

620 in equation (2). This approximation is a modification of Manning's formula for flow in gullies. According to Foster G.R. (1984), the values of ε and e_1 are 0.5 and 0.64, respectively. The non-linear

equation (3) corresponds to an adaptation of Kubota and Sivapalan (1995) formula for subsurface runoff.

$$v_2 = \frac{\varepsilon}{n} S_0^{1/2} A_2(t)^{(2/3)e_1}$$

625

$$v_3 = \frac{K_s S_o^2}{(b+1)A_g^b} A_3(t)^b$$

Where k_s is the saturated hydraulic conductivity, and b is dependent on the soil type, and it is assumed equal to 2. A_g is the equivalent cross-section area to the maximum gravitational storage (H_g). There is also return flow from tank 3 to tank 2 when $S_3 = H_g$, representing runoff generation

630   by saturation.

The equations describe the momentum of a kinematic wave approximation. In both cases, velocity depends on the tank storage. These relations could be summarized by the equation (1), that could be solved numerically coupled with a mass balance equation (4). This equation takes into account the storage at each time step ($S_{tank}(t)$), the longitude of the element (Δx), the time step size (Δt), and

635   the speed estimated for the flow in the time step ($v_{tank}(t)$). Equation (4) is related to equation (1) through the velocity term (v_{tank}) and the cross-sectional area (A). The solution to v_{tank} and A is obtained through an iterative scheme. The total outflow from the tank is calculated using equation (5).

$$A(t) = \frac{S_{tank}(t)}{\Delta x + v_{tank}(t)\Delta t}$$

640

$$E_{tank}(t) = A(t)v_{tank}(t)\Delta t$$

elevation.

4   Results

The primary results of the present study include the reconstruction of the 2015 Salgar flash flood,

645   the assessment of the importance of soil moisture in the hydrologic response of the basin, and the evaluation of the relative role of stratiform and convective precipitation cores in the generation of the observed extreme event. This section is based on the results from the analysis of the hydrological simulation, as well as shallow landslides and flash floods occurrence and simulation.

650   Figure 5a presents the temporal evolution of the convective-stratiform rainfall partitioning during both Events 1 and 2. The main difference between both events is the timing of the convective versus stratiform participation within each case. Event 1 started as a stratiform precipitation event

25

4.1   Hydrologic model validation and sensitivity analysis

Figure 8a presents the results of the hydrological simulation at the outlet of the basin. The model simulation is set to reach a base flow of 3 ~~m^3/s~~ m^3s^{-1}, a value that corresponds to the discharge measurements during field campaigns days and weeks after the flash flood event and during dry

680   spells. The simulation shows that Event 1 generates a hydrograph with a peak flow of $Q_{max} = 160$ ~~m^3/s that did not result in casualties or infrastructure losses, but~~ m^3s^{-1}. It is important to note that during precipitation Event 1 there were no damage nor flooding reports by local authorities. Even though this precipitation event did not generate flooding, it set wet conditions in the entire basin before the occurrence of Event 2 (see the purple line in Figure 8b). Additionally, it is clear

685   from the simulation that during the flash flood event the two successive convective cores over the same region (training convection) generated a peak flow of $Q_{max} =220$ ~~m^3/s~~ m^3s^{-1}, value that is in the upper range of the estimated streamflow based on ~~a posteriori~~ post-event field evidence (185-222 ~~m^3/s~~ m^3s^{-1}). Figure 8a also presents the simulated runoff and subsurface flow separation as
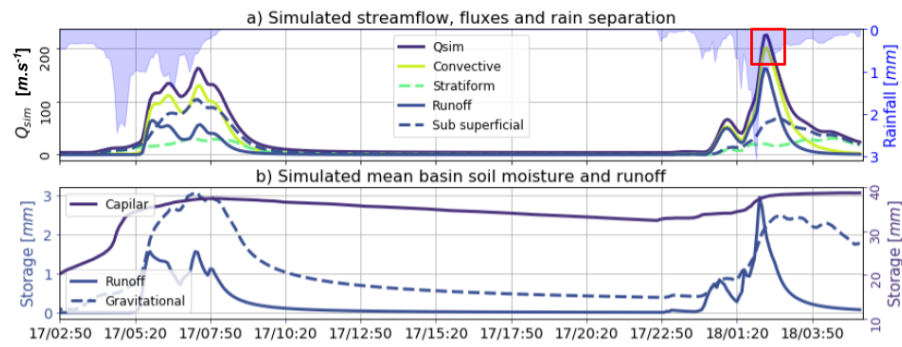
26

Figure 8. Summary of the Results from the hydrological simulation. a) Simulated streamflow, runoff and sub-surface flow separation and convective-stratiform generated discharge discrimination. The red square represents the flash flood peakflow interval estimated based on field campaing evidence. b) Mean runoff, gravitational, and capillary storages during the simulation period.

well as the convective-stratiform generated discharge discrimination. The modeling evidence during
690 Event 2 suggests the convective rainfall fraction dominates the hydrograph formation. In both events, convective (stratiform) precipitation appears to be closely related to the simulated runoff (subsurface flow). On the other hand, the simulated subsurface flow is more important in magnitude than runoff in describing Event 1, while runoff is more relevant for Event 2.

~~Summary of the Results from the hydrological simulation. a) Simulated streamflow, runoff and~~
695 ~~sub-superficial flow separation and convective-stratiform generated discharge discrimination. b) Mean~~
~~runoff, gravitational, and capillary storages during the simulation period.~~

Figure 8b presents capillary storage (purple), as well as runoff (continuous blue) and gravitational (dashed blue) storage temporal variability. As expected, runoff storage is only non-zero during the storm duration, while gravitational storage increases considerably during rain events, followed by a
700 slow recession. There is an increment of basin-wide capillary storage during Event 1, remaining considerably high the time leading to the occurrence of Event 2. According to the model simulations, the peak flow occurred around 2:20 a.m. on May 18th, which is very accurate compared to the reports from local authorities considering all the data limitations.

705 Figure 9 shows the results of a sensitivity analysis of the hydrological simulation during the second rainfall event, varying the infiltration rate, and the surface and subsurface speed parameters. The aim of the sensitivity analysis is to evaluate the robustness of the overall results, considering the fact that the quality and quantity of some of the watershed information is limited. The overall simulation sensitivity results show the main findings described in the previous paragraphs are, in
710 fact, robust to almost all changes in the mentioned parameters, with surface runoff associated with convective rainfall controlling the magnitude of the peak discharge during the Event 2. Changes in the infiltration rate (Figure 9a) result in peak flow changes with a magnitude less than 7%,
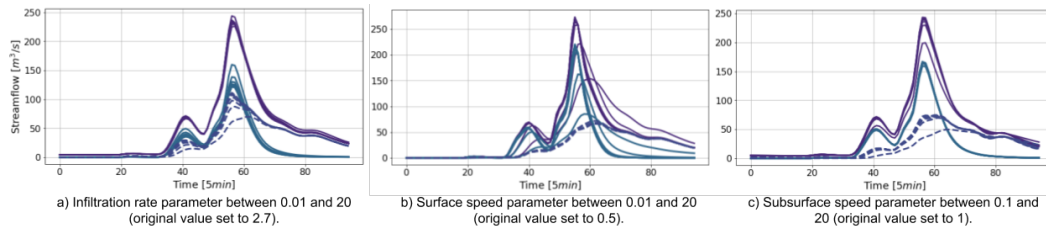
27

Figure 9. Hydrological simulation sensitivity analysis. Similarly as in Figure 8, all panels show the simulated streamflow, and the runoff and sub-surface flow separation. The left panel shows sensitivity to changes in the infiltration rate parameter, the middle panel to changes in surface speed, and the right panel to changes in subsurface speed.

and changes in the subsurface velocity parameter (Figure 9c) lead to peak flow changes with a magnitude less than 20% the original simulation. The model highest sensitivity, and hence the largest uncertainty source, appears to be related to the surface speed parameter (Figure 9b), particularly in the low-end values. Although some of the surface speed values used in the analysis are unrealistically low, it is noteworthy to report that these values lead to the attenuation of the hydrograph and the reduction of the peak flow.

Figure 10 shows the temporal evolution of discharge during Event 2 in different locations along the watershed's main channel. The upper location corresponds to 15% of the area of the basin, and the other downstream locations to 52%, 76%, and 100% of the watershed, respectively. In terms of volume, 73 Mm^3 of the total 144 Mm^3 simulated at the outlet of the basin are generated on the 15% upstream part of the watershed, corresponding to about half of the total mass. In terms of peak flow, due to the slope and velocity changes, the simulated discharge at the 15% upstream part of the watershed corresponds to 61% of the peak discharge at the outlet of the basin.

4.2 Flash flood processes

In this study, we propose a graphical method to assess the soil-rainfall-discharge coupling holistically. The first step is to classify all the cells within the watershed in a predetermined number of groups according to their localization and the distance to the outlet. The aim is to establish a coherent and robust spatial discretization, thus allowing to summarize the concurrent spatio-temporal variability of the different processes in 2D diagrams. Figure ?? presents an example of the spatial structure of cell grouping for La Liboriana basin using 10 (left) and 50 (right) groups.
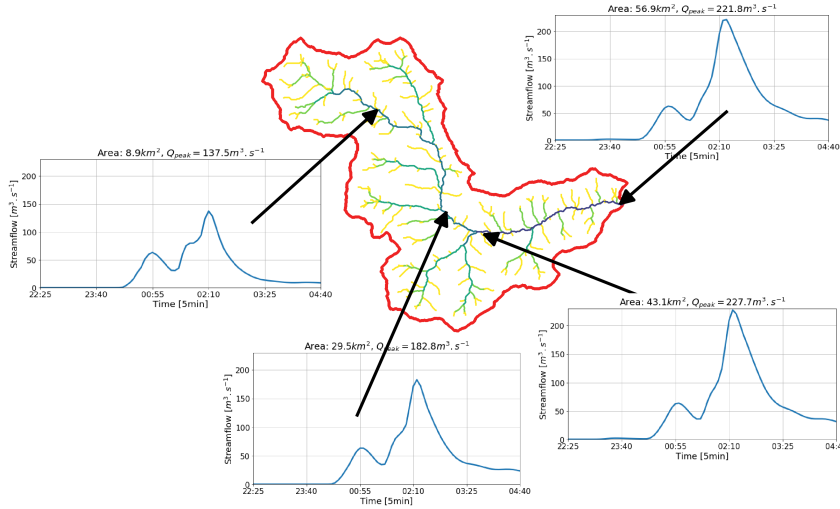
Figure 10. Temporal evolution of discharge during Event 2 in different locations along the watershed's main channel. The upper location corresponds to 15% of the area of the basin, and the other downstream locations to 52%, 76%, and 100% of the watershed, respectively.

~~Example of watershed grouping as a function of distance to the outlet for La Liboriana basin. The left panel corresponds to clustering using ten different groups, and the right panel shows the 50-groups categorization used in the present study.~~

Figure 11 presents the proposed 2D diagrams obtained for the simulation of the La Liboriana basin flash flood using a spatial discretization with 50 groups. Figure 11a includes the evolution of the average rainfall over the basin (black line), and the spatio-temporal evolution of capillary storage (filled isolines) and return flow (colored isolines from white to red) by groups. For the analysis, it is relevant to highlight that higher numbered groups are located away from the outlet of the basin and correspond in this case to considerably steeper slopes. Figure 11b presents the evolution of streamflow at the outlet of the basin (black line) as well as the gravitational storage (filled isolines) and runoff (colored isolines) spatio-temporal evolution. Figure 11 shows variations in the capillary and gravitational storages associated with Event 1 in the higher numbered groups. The capillary storage remains high in almost all the basin until the start of Event 2. According to the conceptualization of the model, the gravitational storage and surface runoff start to interact when the capillary storage is full. In this case, this situation is set up by Event 1. Model runs for Event 2 using dry initial states, show no flooding in the results.
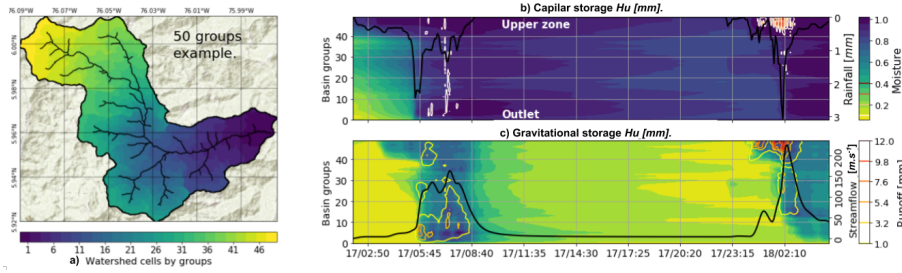
29

Figure 11. ~~Spatiotemporal~~ Watershed groups and spatiotemporal analysis of Events 1 and 2. a) Example of watershed grouping as a function of of their localization and distance to the outlet for La Liboriana basin using a 50-groups categorization. Each group corresponds to a row in the contour plots b) and c). b) Simulated capillary moisture (filled green-to-blue contours) and returned flow occurrence (white to red isolines). The black line represents the average rainfall over the basin. ~~b~~c) Simulated gravitational moisture (filled green-to-blue contours) and runoff (yellow-to-red isolines). The black line represents streamflow at the outlet of the basin. The green-to-blue color bar serves as a reference for capillary moisture and gravitational water content.

It is well known that the temporal variability of rainfall intensity plays an important role in the hydrograph structure. During Event 1 rainfall accumulated over the basin at a relatively stable rate (Figure 12a). On the other hand, Event 2 presents a significant increase in rainfall rate in the second half of the life cycle (Figure 12b). This change in precipitation intensity is associated with a considerable intensification of the training convective cores due to orographic effects. Events 1 and 2 also exhibit differences in the elapsed time between rainfall occurrence and streamflow increment given the relative timing of stratiform versus convective rainfall (see the gray band in Figure 12a and b). For Event 1, the median elapsed time between rainfall and streamflow (Et_{p50}) is 1.12 hours while for Event 2 Et_{p50} is 0.79 hours. The median elapsed time between the convective portion and the streamflow (Etc_{p50}) in Event 1 is 0.75 and 0.46 in Event 2. The minimum value of the convective elapsed time Etc_{min} also descends from 0.42 to 0.25 hours. On the other hand, there is an increase of median elapsed time between stratiform rainfall and streamflow (Ets_{p50}) from 1.21 to 1.83 hours. In Event 2, the convective rainfall and the runoff show a similar evolution, denoting a strong influence of the convective portion (Figure 12b).

As mentioned before, average rainfall accumulation over the basin for Events 1 and 2 is $47mm$ and $38mm$, respectively. During Event 1 (2), convective (stratiform) average accumulations are 28 (23) and 17 (14) mm, respectively (Figure 13a and b). The maximum rainfall intensities are relatively similar with $150mm/h$ and $180mm/h$ for Events 1 and 2, respectively. Despite this, Event 1 does not trigger a flash flood event. The overall evidence suggests that the discriminating factor between both events does not lie in the portions of convective or stratiform rainfall but rather in their spatial distribution.
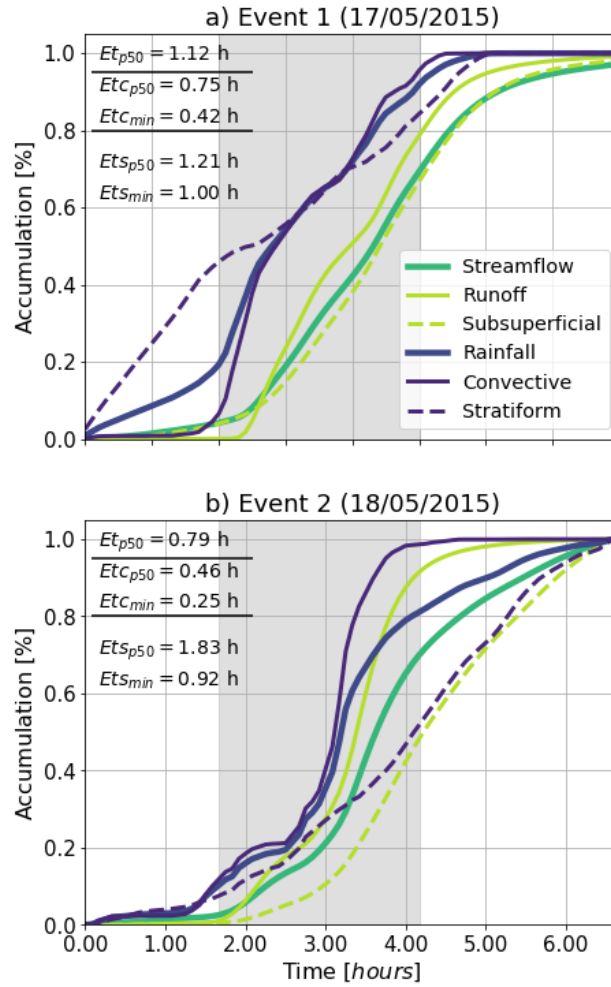
30

Figure 12. Accumulated rainfall and streamflow for a) Event 1 and b) Event 2. The accumulation is expressed in percentage respect to the total value in each case. Median elapsed time and minimum elapsed time () are estimated between total (Et_{p50}, Et_{min}), convective (Etc_{p50}, Etc_{min}), and stratiform (Ets_{p50}, Ets_{min}) rainfall and the runoff portion of the streamflow. Gray bands correspond to the periods for elapsed time estimation.

Figures 13a and b, and Figures 13c and d show the convective and stratiform cumulative rainfall, and the spatially-averaged convective and stratiform rainfall, both as a function of sub-basin reach, respectively. Figures 13a and b show that while Event 1 exhibit similar convective and stratiform rainfall accumulation for different watershed scales, Event 2 shows a more significant cumulative contribution of convective rainfall than of stratiform precipitation. Convective rainfall tends to cover less area, and at the same time present a spatio-temporal erratic behavior (Steiner et al., 1995; Houze, 1989). Figures 13c and d provide evidence that convective rainfall present higher variations at small sub-basins than for a larger-order basin. During Event 2, convective accumulation reaches higher values for small and medium sub-basins. Convective rainfall occurrence at the upper sub-basins
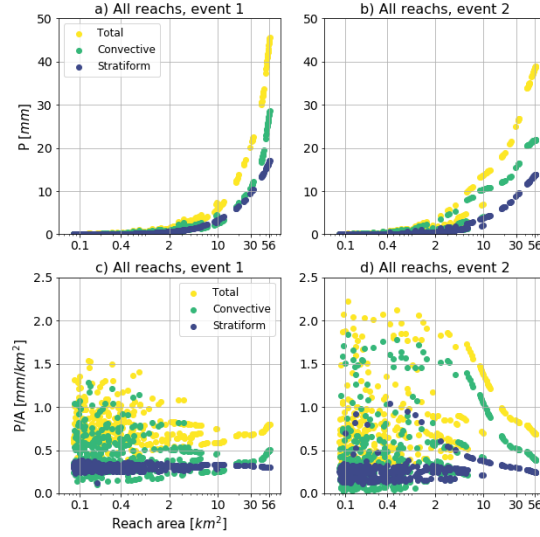
31

Figure 13. Cumulative rainfall versus the area at each reach of the basin for a) Event 1 and b) 2. Panels c) and d) show the average rainfall versus the area at each reach of the basin. Yellow dots correspond to the total, green dots to convective and blue dots to stratiform rainfall. All panels use a logarithmic scale for the basin area.

has significant implications due to geomorphological conditions associated to zero-order sub-basins (Sidle et al., 2018). Figure 14 presents Pearson correlations coefficients between the convective and stratiform hydrograph portions and the runoff and subsurface flow. According to this, convective and stratiform rainfall exhibit a weaker relationship with the flow characteristics at small scales (under $5km^2$). This is likely to be associated with increasing variability of rainfall and hydrograph formation at small scales (Ayalew et al., 2014). Correlations tend to grow with increasing area, indicating stabilization of the hydrograph formation. Additionally, subsurface flow presents higher correlations during Event 1, while correlations with runoff are higher for Event 2, highlighting the most important process in each case. The relevance of subsurface flow is likely due to the rainfall characteristics during Event 1, with homogeneous rainfall intensity and high rate of basin recharge (see Figure 8b). On the other hand, saturation processes and a wet soil profile explain the observed higher correlations during Event 2.

4.3 Landslide and ~~Flood Simulations~~flood simulations

In addition to the hydrological simulation, associated hazards such as floods and landslides are also modeled and discussed in this study. The landslides model as described in the previous section requires additional information including soil depth Z, cohesion C', friction angle ϕ and specific
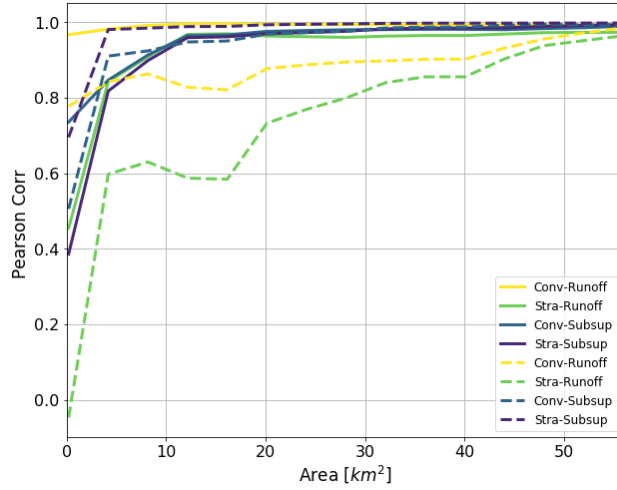
Figure 14. Pearson correlations among convective and stratiform portions of the rainfall and runoff and subsurface flow for different reach areas. Dashed lines correspond to Event 1 and continuous lines Event 2.

weight γ. According to the description by Osorio (2008), illustrating a clay-slime soil, C' is assumed equal to $4KN$, ϕ to 30^0 and γ to 18; Z vary with slope according to Table 1.

805   Figure 15a presents the observed landslides triggered by Event 2 based on aerial photos and satellite images (Landsat/Copernicus, and Google) taken before and after the flash flood. Figure 15b shows, by hills, the map of total unstable cells during the simulation period, and Figure 15c shows the time series of the number of simulated unstable cells during Event 2 (continuous purple line) and the mean rainfall over the basin (inverse axes, blue line). Calibration of the landslide model was per-

810   formed by finding the maximum overlap between simulated and observed unstable and stable cells, and at the same time reducing the overall number of false positives and false negatives. It is important to note that the calibration strategy is not a cell-by-cell modification of the parameters involved but rather a basin-wide modification of soil properties. A sensitivity analysis of soil parameters is carried out by making small variations of the variables within specified intervals: ϕ between 25 and

815   32, γ between 17 and 19, C' between 3.5 and 4.2, and Z between 0.1 and 3 m . The sensitivity analysis suggests that slight variations in the parameter in Z produce significant changes in the modeled landslides, resulting in an overestimation of the number of unstable cells, or no unstable cells at all. Following Table 1, the average soil depth in the basin is only 0.3 m, a value that corresponds to underestimation according to the inspections during field visits. For this reason, the results presented in

820   Figure 15 use a Z map scaled by a calibration factor of 3.5, preserving the spatial dependence on the slope, but achieving a more realistic soil depth and better spatial distribution of landslide occurrence.
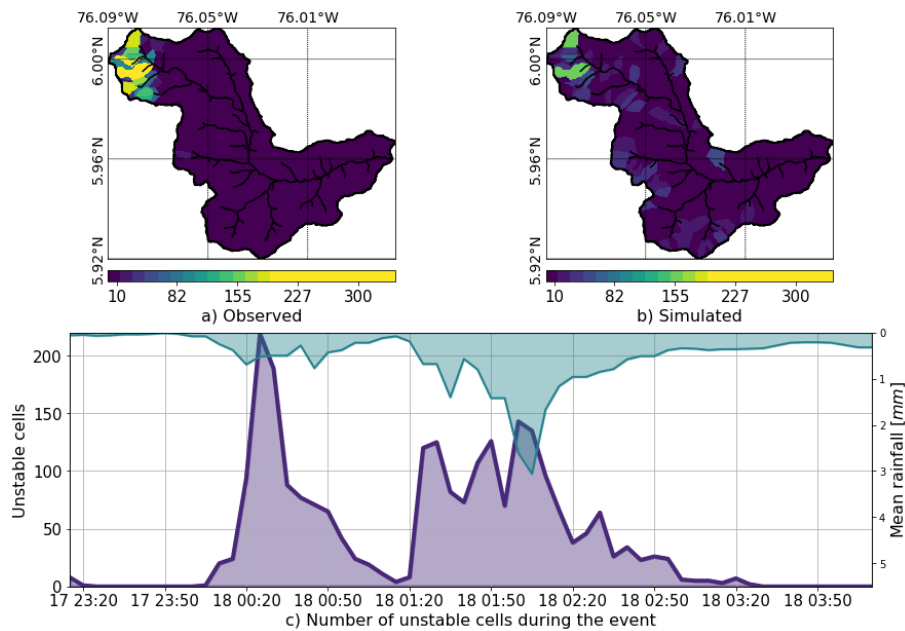
33

Figure 15. a) Observed landslides triggered by Events 1 and 2. The figure is based on aerial photos and satellite images (Landsat/Copernicus, and images available on Google) taken before and after the flash flood event. b) Map of total unstable cells during the simulation period. c) Time series of number of simulated unstable cells during Event 2 (continuous purple line) and mean rainfall over the basin (inverse axes, blue line).

The model represents considerably well the spatial distribution of the areas that are prone to trigger shallow landslides during Event 2, showing a significant density of unstable cells in the hills

825   where slides took place. However, despite the calibration efforts, the total number of unstable cells is relatively low compared to observations. It is important to note that there was no spatial calibration in order to obtain the right location of the landslides. The calibration only includes the change of the soil depth using a single scalar, constant for the entire basin, in order to maximize the number matching observed and simulated slides. In other words, there is just one single basin-wide parameter

830   modified, and not an independent modification of the parameter for every pixel in order to obtain the right distribution. This is important because in that sense, it serves to check the capability of the model to estimate risk areas only considering topography and rainfall data. A pinpoint localization of the unstable cells is still considered a hard task in part due to the small temporal and spatial scale at which landslide processes take place (Aristizábal et al., 2016; Dhakal and Sidle, 2004; Wu and

835   Sidle, 1995). Additionally, the lack of detailed soil information increases the simulation uncertainty. Notwithstanding the difficulties, the results suggest that the model simulations could have been used and should be used in the future for early detection and warning to improve both short and long-term risk reduction strategies.

34

840 ~~According to the model results, a significant portion of the landslides happened during the first of the training convective cores reaching the upper basin (see Figure 15c). Due to the high soil moisture, cells located in the mentioned region where prone to failure. The second and more intense convective core, between 1:20 and 2:15 a.m., also triggered additional slides for an extended period. During storm events, shallow landslides become a significant source of gravels and sediments.~~

845 ~~These particles tend to reach the river network, increasing the magnitude of the streamflow and its destructive power. Despite this, there is no current explicit link in the model between the landslides scheme and the hydraulic submodel. Nonetheless, HydroFlash assumes that sediment transport is limited by channel capacity, and not by hillslope supply, which in this case is guaranteed by the elevated number of landslides.~~

850 Figure 16 shows the identification of the flood spots at the peak of Event 2 (May 18th, 2015, 2:00 a.m.) as simulated using HydroFlah. Figures 16b to f present a detail view of the results from the outlet of the basin to the upper region. Cases presented in Figures 16e and f exhibit a satisfactory agreement with observed flood spots (blue shadow). Cases in Figures 16c and d also show a good approximation, but with minor spatial shifts in some sections. The largest spatial differences are ob-

855 served in Figures 16b. At the entrance of the urban zone, the model overestimates the flood spots. The model results indicate that 11% of flood spots happen at elements of order 1 and 2, and, 18, 38 and 32% happen at orders 3, 4 and 5, respectively. This also highlights a coherent geomorphological representation of the flooded channels and hills with the order.

860 ## 5 Discussion

During the morning of May 18th of 2015, ~~1:30 a.m local time,~~ a flash flood occurred in the steep La Liboriana basin, in the municipality of Salgar, Department of Antioquia, Colombia, leaving more than 100 human casualties, 535 houses destroyed, and significant infrastructure loses. ~~The disaster was reported to departmental and national authorities around 2:00 and 2:30 a.m.~~ Due to the lack of

865 local information of soil type, land use and real-time hydrometeorological data, La Liboriana case implies a challenge for flash flood prediction, modeling and, consequently, risk management. The present paper introduces a ~~hydrological~~ hydrologic model-based approach and an integral graphical analysis tool (an integrated spatiotemporal analysis of rainfall evolution, together with soil storages in the basin), not only to simulate and understand all the relevant soil-rainfall-discharge processes

870 that led to the 2015 Salgar flash flood while assessing the associated natural hazards, but also to propose it as a radar QPE-based landslide and flash flood guidance low-cost tool for basins with scarce data and regions with limited resources.
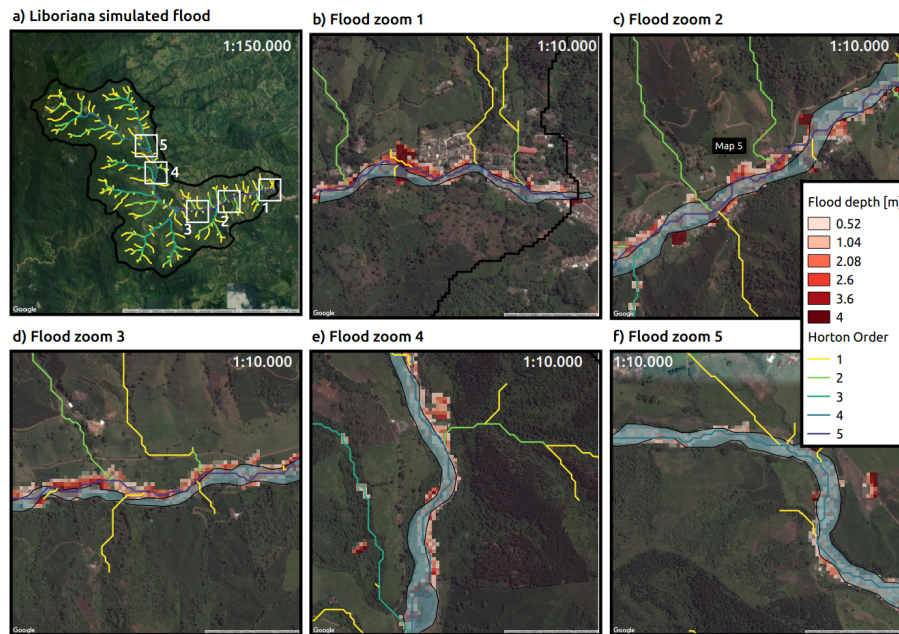
Figure 16. Simulated flood spot at the peak of Event 2 in different locations. a) Basin drainage network. White squares correspond to regions of interest highlighted in panes b) to f). The colors of the streams correspond to the Strahler order of the network. b) Zoom at the outlet of the basin, where an important portion of the human and infrastructure loses took place. c) Zoom at La Margarita settlement also affected by the flash flood. d) to f) Zoom at key locations along the principal stream. Observed flood spots are shown in blue polygons and model flood spots in red to white grids.

The methodology implies the development of a distributed ~~hydrological~~ hydrologic model with the capabilities of tracking independently convective and stratiform precipitation within the model as well as keeping track of the runoff and subsurface portions of the streamflow, coupling a shallow landslide submodel and a one-dimensional flash flood scheme (HydroFlash). The model proposed here indeed allows studying the different hydrological processes relevant to flash flood and landslide occurrence by using different simulation resources, serving as the basis for a better understanding of the overall basin response. This overall approach helps to isolate flood generating mechanisms or causative factors both in time and also in space, focusing on the important physical processes and not only on ~~the~~ statistics (Klemes, 1993; Merz and Blöschl, 2003). It is hoped that knowledge improvement leads to the anticipation of the warning and response by risk management entities.

The evolution of the simulation of Events 1 and 2 show evidence of remarkable behavioral differences. During Event 1 both gravitational and capillary tanks are filled along and across the basin as a result of the quasi-homogeneous rainfall spatial distribution. The return flow is low, and most of the runoff occurs within the first 20 groups (40% of the watershed closest to the outlet). In the

period between both events, there is a recession in the capillary and gravitational storages in the entire basin. Capillary storage decays considerably slower than gravitational storage. During Event 2, the flash flood triggering event, the first convective core saturates both capillary and gravitational storages in the upper part of the basin and generates both return flow and significant runoff. Due to soil saturation, the second convective core results mainly in surface runoff. During this event, runoff is generated the lower part of the basin while extreme runoff rates are evident in the upper part of the basin, collocated with the steeper slopes. On the other hand, subsurface flow is more important in magnitude than runoff describing Event 1, while runoff is more relevant for Event 2. The precedent storage and the presence of thunderstorm training profoundly condition the streamflow during Event 2. The overall evidence suggests that precedent capillary moisture in the basin plays an essential role in modulating river discharge. This behavior could be linked to the temporal occurrence and relative importance and timing of stratiform and convective formations previously described.

While convective and stratiform partitioning could influence the runoff and subsurface flow separation, the spatial distribution of rainfall relative to watershed network morphometry structure impose a condition on the hydrological response of the basin. In other words, hydrograph formation is not only determined by the rainfall accumulation or maximum intensity, but also by its spatial structure. The structure of the rainfall associated with La Liboriana event highlights the need to consider in more detail the role of orographic rainfall intensification in practical applications such as early warning systems. Evidence suggests the spatial structure of the rainfall is at least as important as the geomorphological features of the basin regulating the generation of flash flood events.

An integrated spatiotemporal analysis of rainfall evolution, together with soil storages in the basin is necessary to study the relevance of antecedent conditions and precipitation type, intensity, and location in the generation of flash flood events. Event 1 increased the overall soil moisture with an associated decrease on infiltration rates similar to results reported by Penna et al. (2011) and Zehe et al. (2010), low infiltration increase runoff rates, which finally affects the susceptibility of the basin to flash floods occurrence (Wagner et al., 1999; Penna et al., 2011; Tramblay et al., 2012). La Liboriana geomorphological characteristics, corresponding to a steep tropical basin, determine the potential energy that controls water transit velocity. Water tends to reach faster the channels in order 1 and 2 hills, and, at the same time, the sediment production and transport in these hills tend to be larger. Order 3 sub-basins most likely act as transport elements, with no important energy losses. Floods tend to occur in order 4 and 5 sub-basins due to the widening of the channel and slope attenuation.

Different authors have focused on trying to understand the general causative factors behind the occurrence of flash floods finding similar to our results, a significant role of basing geomorphology,

37

orography and local convection. For example, Lehmann and Or (2012), using a shallow landslide model, finds an important role of the topography and the rainfall conditions. Turkington et al. (2014) shows how intense locally driven convection appears to be the main meteorological trigger for flash occurrence in the French Alps.Camarasa-Belmonte (2016) shows how rainfall intensity and dura-

tion influences the shape of the hydrograph, with intense rainfall shortening the response time of the basin, and large durations increasing the flood peak. In the Mediterranean region, Boudou et al. (2016) states that in addition to the rainfall, geomorphological characteristics and antecedent soil conditions are key in the generation of flash flooding.

However useful, the evidence in this work only takes into account two successive events; an analysis of more cases and different spatial scales (different basins) would provide robust conclusions in this direction. It is clear that it is not conclusive enough to focus on a single extreme event, rather than on a spectrum of floods Merz and Blöschl (2003). The model simulation results suggest it is imperative to study in depth the long-term link between the relative basin and drainage network orientation and the preferred path of precipitation events and its role in defining the frequency of flash flood occurrence. A better understanding of the network-hills-preferential rainfall advection structure could provide information about basins prone to flash floods when information is scarce.

6   Conclusions

Extreme rainfall events such as the one that triggered La Liboriana tragedy frequently take place in Colombia and the entire global tropical belt over ungauged basins, often triggering flash floods and torrential flows, endangering vulnerable communities due to poor long-term planning and lack of functional early warning systems. There is a global need for better knowledge and understanding of the hydrological and meteorological conditions that, combined, lead to the manifestation of natural hazards. Such understanding must result in useful practical applications that improve risk management practices saving lives. In the current work, we approach the problem from a hydrological modeling point of view, trying, despite the data limitations and the uncertainty of the results, to shed some light in the first-order processes that modulate the occurrence of flash floods in the region.

In the case of La Liboriana flash flood, radar reflectivity fields were available from a C-Band radar operated by the Early Warning System of Medellín and its metropolitan area as part of a local risk management strategy. While the municipality of Salgar is located far outside Medellín's metropolitan area, the radar is about 60 90 km away from Salgar, and the reflectivity retrievals enable the classification of precipitation fields into convective and stratiform areas using widely accepted methodologies by the meteorological community. Radar reflectivity is also a proxy for precipita-

38

tion allowing a quantitative estimation of rainfall fields. This estimation was used together with the ~~hydrological modeling~~ hydrologic model to assess the different basin-wide processes taking place during the flash flood triggering rainfall event. The limitations of the methodology presented in this work do not allow to represent all the detailed small-scale preferential pathways of water in the watershed, but rather focus on the first-order approximation to study the partitioning between runoff vs. subsurface flow. Also, the model results are used to obtain a conceptual idea about the general processes, but it must be taken into account that the simulations are subject to a calibration process that could lead to erroneous conclusions about the physical processes. This could be true even as different steps were taken trying to avoid this situation.

The overall model simulation methodology reproduces considerably well the magnitude and timing of La Liboriana flash flood discharge peak, ~~as well as~~ showing robustness to changes in the most important model parameters, and reasonably well the areas of regional land-slide occurrence and flood spots location. ~~Simulation~~ Model simulation results indicate that the flash-flood and the regional land-slide features were strongly influenced by the observed antecedent rainfall associated with a northeasterly stratiform event that recharged the gravitational and capillary storages in the entire basin. The hydrologic simulation shows that the antecedent event set wet conditions in the entire basin before the occurrence of the flash flood event, governing the streamflow during the latter. ~~The~~ Results of the model simulation also suggest that the first of the two successive convective cores (thunderstorm training) over the same region during the second precipitation event (the flash flood event) saturated both capillary and gravitational storages in the upper part of the basin and generated both return flow and significant runoff. The second convective core resulted mainly in surface runoff spatially collocated with the steeper slopes, generating the kinetic energy needed to produce La Liboriana flash flood. Overall results also show ~~an excellent~~ a good agreement between the simulated flood spots and the observed ones; this in spite of the limitations imposed by the resolution of the DEM used for extracting cross sections, and the model ~~simplifications described in the Methodology section~~oversimplifications.

~~The~~ Considering all the shortcomings and generalizations, the described model-based approach is ~~useful to isolate~~ potentially useful to assess flood generating mechanisms and as a tool for policy-makers, not only for short-term decisions in the context of an early warning system but also as a planning resource for long-term risk management. While several improvements ~~could~~ need to be implemented, including a better representation of hydraulic parameters, and a direct link between landslides and flood spots similar to the strategy presented in the STEP-TRAMM model (Fan et al., 2017), the results suggest it is possible to use ~~the~~ low-cost ~~methodology introduced here to not only improve our understanding of hydrological processes but also~~ methodologies such as the one introduced here as a risk management tool in countries and regions with scarce re-

sources.~~In the case of Salgar, there was radar information available, but in many cases, the only near-real-time precipitation information comes from satellite retrievals. It would be very useful from a practical point of view to assess in which cases satellite information is enough for risk management applications. Comparing the Salgar case with the Mocoa (Department of Putumayo, Colombia) April 1st, 2017 flash flood that resulted in more than 330 fatalities could help address this question.~~

7 Acknowledgements

40

References

1020   Adamovic, M., Branger, F., Braud, I., and Kralisch, S.: Development of a data-driven semi-distributed hydro-logical model for regional scale catchments prone to Mediterranean flash floods, Journal of Hydrology, 541, 173–189, doi:10.1016/j.jhydrol.2016.03.032, http://dx.doi.org/10.1016/j.jhydrol.2016.03.032, 2016.

Aristizábal, E., Vélez, J. I., Martínez, H. E., and Jaboyedoff, M.: SHIA_Landslide: a distributed conceptual and physically based model to forecast the temporal and spatial occurrence of shallow landslides triggered

1025   by rainfall in tropical and mountainous basins, Landslides, 13, 497–517, doi:10.1007/s10346-015-0580-7, 2016.

Aronica, G. T., Brigandí, G., and Morey, N.: Flash floods and debris flow in the city area of Messina, north-east part of Sicily, Italy in October 2009: The case of the Giampilieri catchment, Natural Hazards and Earth System Science, 12, 1295–1309, doi:10.5194/nhess-12-1295-2012, 2012.

1030   ASF, J.: Dataset: ASF DAAC 2015, ALOS PALSAR Radiometric Terrain Corrected high res; Includes Material JAXA/METI 2007, doi:10.5067/Z97HFCNKR6VA, https://vertex.daac.asf.alaska.edu/, 2011.

Ayalew, T. B., Krajewski, W. F., and Mantilla, R.: Connecting the power-law scaling structure of peak-discharges to spatially variable rainfall and catchment physical properties, Advances in Water Resources, 71, 32–43, doi:10.1016/j.advwatres.2014.05.009, http://dx.doi.org/10.1016/j.advwatres.2014.05.009, 2014.

1035   Berne, A. and Krajewski, W.: Radar for hydrology: Unfulfilled promise or unrecognized potential?, Advances in Water Resources, 51, 357 – 366, doi:https://doi.org/10.1016/j.advwatres.2012.05.005, http://www.sciencedirect.com/science/article/pii/S0309170812001157, 35th Year Anniversary Issue, 2013.

Beven, K.: Kinematic subsurface stormflow, Water Resources Research, 17, 1419–1424, doi:10.1029/WR017i005p01419, 1981.

1040   Beven, K.: Towards integrated environmental models of everywhere: uncertainty, data and modelling as a learning process, Hydrology and Earth System Sciences, 11, 460–467, doi:10.5194/hess-11-460-2007, http://www.hydrol-earth-syst-sci.net/11/460/2007/{%}5Cnhttps://hal.archives-ouvertes.fr/hal-00305631/, 2007.

Bisht, S., Chaudhry, S., Sharma, S., and Soni, S.: Assessment of flash flood vulnerability zonation through Geospatial technique in high altitude Himalayan watershed, Himachal Pradesh India, Remote Sensing Ap-

1045   plications: Society and Environment, 12, 35–47, doi:10.1016/j.rsase.2018.09.001, https://doi.org/10.1016/j.rsase.2018.09.001, 2018.

Blöschl, G., Sivapalan, M., Wagener, T., Viglione, A., and Savenije, H.: Runoff Prediction in Ungauged Basins, in: Runoff Prediction in Ungauged Basins: Synthesis across Processes, Places and Scales, edited by Blöschl, G., Sivapalan, M., Wagener, T., Viglione, A., and Savenije, H., Cambridge Uni-

1050   versity Press, Cambridge, https://www.cambridge.org/core/books/runoff-prediction-in-ungauged-basins/runoff-prediction-in-ungauged-basins/A5DFE99C3CA857127C4C03C6C20032EE, 2012.

Bonell, M., McDonnell, J. J., Scatena, F. N., Seibert, J., Uhlenbrook, S., and van Lanen, H. A. J.: HELPing FRIENDs in PUBs: Charting a course for synergies within international water research programmes in gauged and ungauged basins, Hydrological Processes, 20, 1867–1874, doi:10.1002/hyp.6196, 2006.

1055   Borga, M., Anagnostou, E. N., Blöschl, G., and Creutin, J. D.: Flash flood forecasting, warning and risk management: The HYDRATE project, Environmental Science and Policy, 14, 834–844, doi:10.1016/j.envsci.2011.05.017, 2011.

Borga, M., Stoffel, M., Marchi, L., Marra, F., and Jakob, M.: Hydrogeomorphic response to extreme rainfall in headwater systems: Flash floods and debris flows, Journal of Hydrology, 518, 194–205, doi:10.1016/j.jhydrol.2014.05.022, http://dx.doi.org/10.1016/j.jhydrol.2014.05.022, 2014.

Boudou, M., Lang, M., Vinet, F., and C??ur, D.: Comparative hazard analysis of processes leading to remarkable flash floods (France, 1930???1999), Journal of Hydrology, 541, 533–552, doi:10.1016/j.jhydrol.2016.05.032, http://dx.doi.org/10.1016/j.jhydrol.2016.05.032, 2016.

Braud, I., Borga, M., Gourley, J., H??rlimann, M., Zappa, M., and Gallart, F.: Flash floods, hydro-geomorphic response and risk management, Journal of Hydrology, 541, 1–5, doi:10.1016/j.jhydrol.2016.08.005, http://dx.doi.org/10.1016/j.jhydrol.2016.08.005, 2016.

Camarasa-Belmonte, A. M.: Flash floods in Mediterranean ephemeral streams in Valencia Region (Spain), Journal of Hydrology, doi:10.1016/j.jhydrol.2016.03.019, 2016.

Castillo, V. M., Gómez-Plaza, A., and Martínez-Mena, M.: The role of antecedent soil water content in the runoff response of semiarid catchments: A simulation approach, Journal of Hydrology, 284, 114–130, doi:10.1016/S0022-1694(03)00264-6, 2003.

Cea, L. and Blade, E.: A simple and efficient unstructured finite volume scheme for solving the shallow water equations in overland flow applications, Water Resources Research, 51, 5464–5486, doi:10.1002/2014WR016259, 2015.

Creutin, J. D. and Borga, M.: Radar hydrology modifies the monitoring of flash-flood hazard, Hydrological Processes, 17, 1453–1456, doi:10.1002/hyp.5122, 2003a.

Creutin, J. D. and Borga, M.: Radar hydrology modifies the monitoring of flash-flood hazard, Hydrological Processes, 17, 1453–1456, doi:10.1002/hyp.5122, 2003b.

Dhakal, A. S. and Sidle, R. C.: Distributed simulations of landslides for different rainfall conditions, Hydrological Processes, 18, 757–776, doi:10.1002/hyp.1365, 2004.

Douinot, A., Roux, H., Garambois, P. A., Larnier, K., Labat, D., and Dartus, D.: Accounting for rainfall systematic spatial variability in flash flood forecasting, Journal of Hydrology, 541, 359–370, doi:10.1016/j.jhydrol.2015.08.024, http://dx.doi.org/10.1016/j.jhydrol.2015.08.024, 2016.

Duan, Q., Schaake, J., Andreassian, V., Franks, S., Goteti, G., Gupta, H., Gusev, Y., Habets, F., Hall, a., Hay, L., Hogue, T., Huang, M., Leavesley, G., Liang, X., Nasonova, O., Noilhan, J., Oudin, L., Sorooshian, S., Wagener, T., and Wood, E.: Model Parameter Estimation Experiment (MOPEX): An overview of science strategy and major results from the second and third workshops, Journal of Hydrology, 320, 3–17, doi:10.1016/j.jhydrol.2005.07.031, 2006.

(eds.), D. C. A. D. I.: Severe Convective Storms, Meteorological Monographs, American Meteorological Society, http://gen.lib.rus.ec/book/index.php?md5=7AEF0E8299AB41644901046180BED4FC, 2001.

Fan, L., Lehmann, P., McArdell, B., and Or, D.: Linking rainfall-induced landslides with debris flows runout patterns towards catchment scale hazard assessment, Geomorphology, 280, 1–15, doi:10.1016/j.geomorph.2016.10.007, http://dx.doi.org/10.1016/j.geomorph.2016.10.007, 2017.

Foster G.R., Huggins L.F., M. L.: A Laboratory Study of Rill Hydraulics: I. Velocity Relationships, American Society of Agricultural and Biological Engineers, 3, 0790–0796, doi:10.13031/2013.32873, 1984.

Fragoso, M., Trigo, R. M., Pinto, J. G., Lopes, S., Lopes, a., Ulbrich, S., and Magro, C.: The 20 February 2010 Madeira flash-floods: Synoptic analysis and extreme rainfall assessment, Natural Hazards and Earth System Science, 12, 715–730, doi:10.5194/nhess-12-715-2012, 2012.

Francés, F., Vélez, J. I., and Vélez, J. J.: Split-parameter structure for the automatic calibration of distributed hydrological models, Journal of Hydrology, 332, 226–240, doi:10.1016/j.jhydrol.2006.06.032, 2007a.

Francés, F., Vélez, J. I., and Vélez, J. J.: Split-parameter structure for the automatic calibration of distributed hydrological models, Journal of Hydrology, 332, 226–240, doi:10.1016/j.jhydrol.2006.06.032, 2007b.

Garambois, P. a., Roux, H., Larnier, K., Castaings, W., and Dartus, D.: Characterization of process-oriented hydrologic model behavior with temporal sensitivity analysis for flash floods in Mediterranean catchments, Hydrology and Earth System Sciences, 17, 2305–2322, doi:10.5194/hess-17-2305-2013, 2013.

Gibson, S., Park, H. J., and Fleming, M.: Modeling Watershed and Riverine Sediment Processes with HEC-HMS and HEC-RAS, Watershed Management, pp. 1340–1349, 2010.

Gochis, D., Schumacher, R., Friedrich, K., Doesken, N., Kelsch, M., Sun, J., Ikeda, K., Lindsey, D., Wood, A., Dolan, B., Matrosov, S., Newman, A., Mahoney, K., Rutledge, S., Johnson, R., Kucera, P., Kennedy, P., Sempere-Torres, D., Steiner, M., Roberts, R., Wilson, J., Yu, W., Chandrasekar, V., Rasmussen, R., Anderson, A., and Brown, B.: The great Colorado flood of September 2013, Bulletin of the American Meteorological Society, 96, 1461–1487, doi:10.1175/BAMS-D-13-00241.1, 2015.

Golden, L. A. and Springer, G. S.: Channel geometry, median grain size, and stream power in small mountain streams, Geomorphology, 78, 64–76, doi:10.1016/j.geomorph.2006.01.031, 2006.

Gruntfest, E. and Handmer, J.: Coping with Flash Floods, NATO science series. Partnership sub-series 2, Environmental security, Springer Netherlands, https://books.google.com.co/books?id=pwsczTbbY9sC, 2001.

Hardy, J., Gourley, J. J., Kirstetter, P. E., Hong, Y., Kong, F., and Flamig, Z. L.: A method for probabilistic flash flood forecasting, Journal of Hydrology, 541, 480–494, doi:10.1016/j.jhydrol.2016.04.007, http://dx.doi.org/10.1016/j.jhydrol.2016.04.007, 2016.

Houze, R.: Mesoscale convective systems, Reviews of Geophysics, 42, doi:10.1029/2004RG000150, https://agupubs.onlinelibrary.wiley.com/doi/abs/10.1029/2004RG000150, 2004.

Houze, R. A.: Observed structure of mesoscale convective systems and implications for large-scale heating, Quarterly Journal of the Royal Meteorological Society, 115, 425–461, doi:10.1002/qj.49711548702, 1989.

Houze, R. A., Rasmussen, K. L., Zuluaga, M. D., and Brodzik, S. R.: The variable nature of convection in the tropics and subtropics: A legacy of 16 years of the Tropical Rainfall Measuring Mission satellite, Reviews of Geophysics, 53, 994–1021, doi:10.1002/2015RG000488, 2015.

Jonkman, S.: Global perspectives on loss of human life caused by floods, NATURAL HAZARDS, 34, 151–175, doi:10.1007/s11069-004-8891-3, 2005.

Kahana, R., Ziv, B., Enzel, Y., and Dayan, U.: Synoptic climatology of major floods in the Negev Desert, Israel, International Journal of Climatology, 22, 867–882, doi:10.1002/joc.766, 2002.

Khosravi, K., Pham, B. T., Chapi, K., Shirzadi, A., Shahabi, H., Revhaug, I., Prakash, I., and Tien Bui, D.: A comparative assessment of decision trees algorithms for flash flood susceptibility modeling at Haraz watershed, northern Iran, Science of the Total Environment, 627, 744–755, doi:10.1016/j.scitotenv.2018.01.266, https://doi.org/10.1016/j.scitotenv.2018.01.266, 2018.

1135   Kirkby, M. J. and Chorley, R. J.: Throughflow, Overland Flow and Erosion, International Association of Scientific Hydrology. Bulletin, 12, 5–21, doi:10.1080/02626666709493533, http://www.tandfonline.com/doi/abs/10.1080/02626666709493533, 1967.

Klemes, V.: Probability of extreme hydrometeorological events—A differ- ent approach, in Extreme Hydrological Events: Precipitation, Floods and Droughts, IAHS Publ, 1993.

1140   Kubota, J. and Sivapalan, M.: Towards a Catchment-Scale Model of Subsurface Small-Scale Process-Based Modelling and Runoff Generation Based on Synthesis of Field Studies, Hydrological Processes, 9, 541–554, 1995.

Lehmann, P. and Or, D.: Hydromechanical triggering of landslides: From progressive local failures to mass release, Water Resources Research, 48, 1–24, doi:10.1029/2011WR010947, 2012.

1145   Leopold, L.B., M. T.: The hydraulic geometry of stream channels and some physiographic implications, Geological survey professional paper, 1953.

Llasat, M. C., Marcos, R., Turco, M., Gilabert, J., and Llasat-Botija, M.: Trends in flash flood events versus convective precipitation in the Mediterranean region: The case of Catalonia, Journal of Hydrology, 541, 24–37, doi:10.1016/j.jhydrol.2016.05.040, http://dx.doi.org/10.1016/j.jhydrol.2016.05.040, 2016.

1150   Longoni, L., Ivanov, V. I., Brambilla, D., Radice, A., and Papini, M.: Analysis of the temporal and spatial scales of soil erosion and transport in a Mountain Basin, Italian Journal of Engineering Geology and Environment, 16, 17–30, doi:10.4408/IJEGE.2016-02.O-02, 2016.

Mapes, B., Warner, T., Xu, M., and Negri, A. J.: Diurnal Patterns of Rainfall in Northwestern South America. Part I: Observations and Context, Monthly Weather Review, 131, 799–812, doi:10.1175/1520-

1155   0493(2003)131<0799:DPORIN>2.0.CO;2, https://doi.org/10.1175/1520-0493(2003)131<0799:DPORIN>2.0.CO;2, 2003.

Marchi, L., Cavalli, M., Amponsah, W., Borga, M., and Crema, S.: Upper limits of flash flood stream power in Europe, Geomorphology, 272, 68–77, doi:10.1016/j.geomorph.2015.11.005, http://dx.doi.org/10.1016/j.geomorph.2015.11.005, 2016.

1160   Marra, F., Destro, E., Nikolopoulos, E. I., Zoccatelli, D., Dominique Creutin, J., Guzzetti, F., and Borga, M.: Impact of rainfall spatial aggregation on the identification of debris flow occurrence thresholds, Hydrology and Earth System Sciences, 21, 4525–4532, doi:10.5194/hess-21-4525-2017, 2017.

Martín-Vide, J. P. and Llasat, M. C.: The 1962 flash flood in the Rubí stream (Barcelona, Spain), Journal of Hydrology, 566, 441–454, doi:10.1016/j.jhydrol.2018.09.028, https://doi.org/10.1016/j.jhydrol.2018.09.028,

1165   2018.

Merz, R. and Blöschl, G.: A process typology of regional floods, Water Resources Research, 39, 1–20, doi:10.1029/2002WR001952, http://doi.wiley.com/10.1029/2002WR001952, 2003.

Norbiato, D., Borga, M., Degli Esposti, S., Gaume, E., and Anquetin, S.: Flash flood warning based on rainfall thresholds and soil moisture conditions: An assessment for gauged and ungauged basins, Journal of Hydrol-

1170   ogy, pp. 274–290, doi:10.1016/j.jhydrol.2008.08.023, 2008.

Obrien, J.S., J. P.: Laboratory analysis of mudflow properties, Journal of Hydrological Engineering, 8, 877–887, 1988.

Osorio, H.G., A. S.: Unidades de suelo representativas de la zona cafetera de Colombia, Federación de Cafeteros de Colombia, 2008.

1175 Ozturk, U., Wendi, D., Crisologo, I., Riemer, A., Agarwal, A., Vogel, K., López-Tarazón, J. A., and Korup, O.: Rare flash floods and debris flows in southern Germany, Science of the Total Environment, 626, 941–952, doi:10.1016/j.scitotenv.2018.01.172, 2018.

Penna, D., Tromp-Van Meerveld, H. J., Gobbi, a., Borga, M., and Dalla Fontana, G.: The influence of soil moisture on threshold runoff generation processes in an alpine headwater catchment, Hydrology and Earth

1180 System Sciences, 15, 689–702, doi:10.5194/hess-15-689-2011, 2011.

Peterson, P.: F2PY: a tool for connecting Fortran and Python programs, International Journal of Computational Science and Engineering, 4, 296, doi:10.1504/IJCSE.2009.029165, http://www.inderscience.com/link.php?id=29165, 2009.

Piper, D., Kunz, M., Ehmele, F., Mohr, S., Mühr, B., Kron, A., and Daniell, J.: Exceptional sequence of severe

1185 thunderstorms and related flash floods in May and June 2016 in Germany. Part I: Meteorological background, Natural Hazards and Earth System Sciences Discussions, pp. 1–30, doi:10.5194/nhess-2016-275, http://www.nat-hazards-earth-syst-sci-discuss.net/nhess-2016-275/, 2016.

Poveda, G. and Mesa, O. J.: On the existence of Lloró (the rainiest locality on Earth): Enhanced ocean-land-atmosphere interaction by a low-level jet, Geophysical Research Letters, 27, 1675–1678,

1190 doi:10.1029/1999GL006091, https://agupubs.onlinelibrary.wiley.com/doi/abs/10.1029/1999GL006091, 2000.

Poveda, G., Vélez, J. I., Mesa, O. J., Cuartas, A., Barco, J., Mantilla, R. I., Mejía, J. F., Hoyos, C. D., Ramírez, J. M., Ceballos, L. I., Zuluaga, M. D., Arias, P. a., Botero, B. a., Montoya, M. I., Giraldo, J. D., and Quevedo, D. I.: Linking Long-Term Water Balances and Statistical Scaling to Estimate River Flows along

1195 the Drainage Network of Colombia, Journal of Hydrologic Engineering, 12, 4–13, doi:10.1061/(ASCE)1084-0699(2007)12:1(4), 2007.

Rennó, C. D., Nobre, A. D., Cuartas, L. A., Soares, J. V., Hodnett, M. G., Tomasella, J., and Waterloo, M. J.: HAND, a new terrain descriptor using SRTM-DEM: Mapping terra-firme rainforest environments in Amazonia, Remote Sensing of Environment, 112, 3469–3481, doi:10.1016/j.rse.2008.03.018,

1200 http://linkinghub.elsevier.com/retrieve/pii/S003442570800120X, 2008.

Rodriguez-Blanco, M., Taboada-Castro, M., and Taboada-Castro, M.: Rainfall–runoff response and event-based runoff coefficients in a humid area (northwest Spain), Hydrological Sciences Journal, 403, 319–329, doi:10.1080/02626669509491418, http://www.tandfonline.com/action/journalInformation?journalCode=thsj20{%}0Ahttp://www.tandfonline.com/action/journalInformation?journalCode=thsj20, 2012.

1205 Roux, H., Labat, D., Garambois, P. A., Maubourguet, M. M., Chorda, J., and Dartus, D.: A physically-based parsimonious hydrological model for flash floods in Mediterranean catchments, Natural Hazards and Earth System Science, 11, 2567–2582, doi:10.5194/nhess-11-2567-2011, 2011.

Ruiz-Villanueva, V., Díez-Herrero, A., Bodoque, J. M., Ballesteros Cánovas, J. A., and Stoffel, M.: Characterisation of flash floods in small ungauged mountain basins of Central Spain using an integrated ap-

1210 proach, Catena, 110, 32–43, doi:10.1016/j.catena.2013.06.015, http://dx.doi.org/10.1016/j.catena.2013.06.015, 2013.

Šálek, M., Brezková, L., and Novák, P.: The use of radar in hydrological modeling in the Czech Republic – case studies of flash floods, Natural Hazards and Earth System Science, 6, 229–236, doi:10.5194/nhess-6-229-2006, 2006.

1215   Savage, S. B. and Sayed, M.: Stresses developed by dry cohesionless granular materials sheared in an annular shear cell, Journal of Fluid Mechanics, 142, 391–430, doi:10.1017/S0022112084001166, 1984.

Schumacher, R. S. and Johnson, R. H.: Organization and Environmental Properties of Extreme-Rain-Producing Mesoscale Convective Systems, Monthly Weather Review, 133, 961–976, doi:10.1175/MWR2899.1, http://journals.ametsoc.org/doi/abs/10.1175/MWR2899.1, 2005.

1220   Seibert, J. and Beven, K. J.: Gauging the ungauged basin : how many discharge measurements are needed?, Hydrology and Earth System Sciences, 13, 883–892, doi:10.5194/hessd-6-2275-2009, http://www.hydrol-earth-syst-sci.net/13/883/2009/, 2009.

Serra, J.: Image Analysis and Mathematical Morphology, Academic Press, Inc., Orlando, FL, USA, 1983.

Shope, C. L.: Disentangling event-scale hydrologic flow partitioning in mountains of the Korean Peninsula

1225   under extreme precipitation, Journal of Hydrology, 538, 399–415, doi:10.1016/j.jhydrol.2016.04.050, http://dx.doi.org/10.1016/j.jhydrol.2016.04.050, 2016.

Sidle, R., Gomi, T., and Tsukamoto, Y.: Discovery of zero-order basins as an important link for progress in hydrogeomorphology, Hydrological Processes, pp. 1–7, doi:10.1002/hyp.13246, http://doi.wiley.com/10.1002/hyp.13246, 2018.

1230   Sivapalan, M., Takeuchi, K., FRANKS, S. W., GUPTA, V. K., KARAMBIRI, H., LAKSHMI, V., LIANG, X., McDONNELL, J. J., MENDIONDO, E. M., J, P. E. O., OKI, T., POMEROY, J. W., SCHERTZER, D., UHLENBROOK, S., and E. ZEHE: IAHS Decade on Predictions in Ungauged Basins (PUB), 2003–2012: Shaping an exciting future for the hydrological sciences, Hydrological Sciences Journal, pp. 857–880, doi:10.1080/02626667.2015.1131899, http://www.tandfonline.com/action/

1235   journalInformation?journalCode=thsj20{%}5Cnhttp://dx.doi.org/10.1080/02626667.2015.1131899, 2016.

Steiner, M., Houze, R. a., and Yuter, S. E.: Climatological Characterization of Three-Dimensional Storm Structure from Operational Radar and Rain Gauge Data, doi:10.1175/1520-0450(1995)034<1978:CCOTDS>2.0.CO;2, papers3://publication/uuid/D11C9905-6CE2-40B5-8A93-5E5300EB3A6E, 1995.

1240   Takahashi, T.: Debris flow, Taylor y francis, 2 edn., 1991.

Tramblay, Y., Bouaicha, R., Brocca, L., Dorigo, W., Bouvier, C., Camici, S., and Servat, E.: Estimation of antecedent wetness conditions for flood modelling in northern Morocco, Hydrology and Earth System Sciences, 16, 4375–4386, doi:10.5194/hess-16-4375-2012, 2012.

Turkington, T., Ettema, J., Van Westen, C. J., and Breinl, K.: Empirical atmospheric thresholds for debris flows

1245   and flash floods in the southern French Alps, Natural Hazards and Earth System Sciences, 14, 1517–1530, doi:10.5194/nhess-14-1517-2014, 2014.

Vannier, O., Anquetin, S., and Braud, I.: Investigating the role of geology in the hydrological response of Mediterranean catchments prone to flash-floods: Regional modelling study and process understanding, Journal of Hydrology, 541, 158–172, doi:10.1016/j.jhydrol.2016.04.001, http://dx.doi.org/10.1016/j.jhydrol.

1250   2016.04.001, 2016.

Vélez, J.: Desarrollo de un modelo hidrológico conceptual y distribuido orientado a la simulación de crecidas, Tesis doctoral - Universidad Politécnica de Valencia, p. 266, 2001.

Wagener, T., Gupta, H., Yatheendradas, S., Goodrich, D., Unkrich, C., and Schaffner, M.: Understanding sources of uncertainty in flash-flood forecasting for semi-arid regions., IAHS Publication 313, pp. 204–212, 2007.

Wagner, W., Lemoine, G., and Rott, H.: A method for estimating soil moisture from ERS Scatterometer and soil data, Remote Sensing of Environment, 70, 191–207, doi:10.1016/S0034-4257(99)00036-X, 1999.

Wu, W. and Sidle, R. C.: and Number Values Agreed Closely With, Water Resources, 31, 2097–2110, doi:10.1029/95WR01136, 1995.

Yamanaka, T. and Ma, W.: Runoff prediction in a poorly gauged basin using isotope-calibrated models, Journal of Hydrology, 544, 567–574, doi:10.1016/j.jhydrol.2016.12.005, http://dx.doi.org/10.1016/j.jhydrol.2016.12.005, 2017.

Yatheendradas, S., Wagener, T., Gupta, H., Unkrich, C., Goodrich, D., Schaffner, M., and Stewart, A.: Understanding uncertainty in distributed flash flood forecasting for semiarid regions, Water Resources Research, 44, 1–17, doi:10.1029/2007WR005940, 2008.

Younis, J., Anquetin, S., and Thielen, J.: The benefit of high-resolution operational weather forecasts for flash flood warning, Hydrology and Earth System Sciences Discussions, 5, 345–377, doi:10.5194/hessd-5-345-2008, 2008.

Zehe, E., Graeff, T., Morgner, M., Bauer, A., and Bronstert, A.: Plot and field scale soil moisture dynamics and subsurface wetness control on runoff generation in a headwater in the Ore Mountains, Hydrology and Earth System Sciences, 14, 873–889, doi:10.5194/hess-14-873-2010, 2010.